# EFFECTS OF ION-PLATING ON LOW CYCLE FATIGUE BEHAVIOR OF COPPER SINGLE CRYSTALS

A THESIS

Presented to

The Faculty of the Division

of Graduate Studies

By

Edmund Yung Chen

In Partial Fulfillment

of the Requirements for the Degree

Doctor of Philosophy

in the School of Mechanical Engineering

Georgia Institute of Technology

July, 1975

EFFECTS OF ION-PLATING ON LOW CYCLE FATIGUE BEHAVIOR OF COPPER SINGLE CRYSTALS

Approved:

E. A. Starke, Jr., Chairman

J. T. Berry

D. Kalish

B. G. LeFevre

H. E. Grenga

Date Approved: July 8, 1975

## ACKNOWLEDGMENTS

The author would like to express his gratitude to all the individuals who have contributed to this work. They are too many to name individually, but the author would like to take this opportunity of expressing his warm thanks to Dr. Edgar A. Starke, Jr., his thesis advisor, who has given most generously of his time and knowledge in the past few years. He would also like to thank Drs. J. T. Berry, D. Kalish, B. G. LeFevre, and H. E. Grenga for their suggestions and criticism.

This work was sponsored by the Air Force Office of Scientific Research under Grant AFOSR-74-2615, whose support is deeply appreciated.

TABLE OF CONTENTS

# LIST OF ILLUSTRATIONS

Figure Page

Figure Page

# LIST OF TABLES

## SUMMARY

Persistent slip bands (PSB), with their characteristic notch-peak topography on the surface, are usually the fatigue crack initiation sites for pure single-phase materials; especially for pure single crystals. The dislocation mechanisms for PSB formation is not completely known, however it is generally agreed that the ease of cross-slip promotes its development. Thus such factors as high stacking fault energy (SFE), high temperature, and high strain amplitudes, all of which promote cross-slip, favor the formation of PSB. The objective of this research was to investigate the effect of the ion-plated coatings of various SFE's on the low cycle fatigue behavior of copper single crystals.

Fatigue and tensile samples were prepared from copper single crystal rods and pure metal films were coated on the surface by the ion-plating technique. The coating materials were nickel and silver, whose SFE's are respectively higher and lower than that of copper. In addition, copper films were coated on copper samples to evaluate the influence of residual stresses and imperfections created by ion plating.

The silver plated crystals showed an increase in fatigue life, while the nickel plated crystals showed a decrease when compared with uncoated or copper coated

crystals. This effect was attributed to crack initiation being either retarded or promoted by the different surface coatings. The copper plated crystals had the same fatigue life as the unplated crystals. Therefore, the surface residual stresses initiated by the strongly adherent ion plated coating could be neglected.

# CHAPTER I

## INTRODUCTION

Metallic coatings have been widely used in industry for controlling corrosion and erosion. The principle of this technique is to separate the metal being protected from the unfavorable surroundings. An improvement arises from the inertness of the coating material with the environment. However, other situations occur if the coated specimen is under static or dynamic loading. In these cases, the surface coating does not merely serve as a protecting element, but it may also change the mechanical properties of the bulk material. The plastic deformation processes of a coated material are influenced by a complicated combination of several strengthening mechanisms. A more detailed discussion will be provided in the next chapter; however they are related to the type of interface formed and the property differences between the coating material and the substrate.

Many coating techniques are now available. They range from the classical hot dipping, metal spraying to the more recent electroplating and vacuum deposition. All of these methods can be roughly divided into two groups: those that create an abrupt interface with a composition discontinuity between the coating surface and the substrate, and

those that create a composition variation at the interface. In the present study, a newly developed ion-plating technique was used. Basically, it consists of sputter etching and ion implantation. By going through these processes, a strongly adherent interface is formed between the coating material and the substrate. A graded interface is created due to the high velocity of ionized particles, however, its thickness is smaller than that obtained by diffusion processes. Consequently, this technique can not be listed distinctively in either of the above mentioned groups.

There is considerable evidence that the mechanical properties and deformation behavior of crystals can be influenced by surface coatings. There are advantages of ion plated coatings over other conventional coatings for applications such as in antifriction and lubrication.[1] However, fatigue, which is a very surface sensitive property, has not been widely studied. It was the chief goal of this research to investigate the low cycle fatigue behavior of copper single crystals, ion-plated with different materials.

Almost all fatigue studies in the past few decades have been conducted in the high-cycle range. The low cycle fatigue range has not been as extensively investigated. Fatigue damage is certainly caused by cyclic plastic strain. The only significant difference between various fatigue ranges is the degree of cyclic plasticity. For high cycle fatigue, the plastic strain is more localized than for low

cycle fatigue and the resulting imperfections are more difficult to analyze. In addition, low cycle fatigue tests offer the advantage of being conducted in a reasonable length of time. Strain controlled fatigue tests were performed. The advantages of strain controlled fatigue tests have been described elsewhere.[2,3]

By using copper single crystals of identical orientation, we hoped to eliminate the influece of many factors and minimize ambiguities which might lead to misinterpretation of the final results. In addition, the fatigue lives of single crystals normally can be reproduced.[4] The coating materials were chosen so as to have quite different stacking fault energies when compared with copper and yet be compatible with respect to crystal system and atomic size. There has been convincing evidence demonstrating the role of stacking fault energy on the fatigue crack initiation period and fatigue crack propagation rate. These factors combined with the fact that fatigue cracks usually initiate on the surface suggested that future studies of single crystals coated with materials of different stacking fault energy might offer ways of controlling fatigue crack initiation. The question of whether the ion plating process itself may generate significant damage on the surface is still unknown. This was also evaluated in this study.

# CHAPTER II

## BACKGROUND

There is considerable evidence that the mechanical properties and the deformation behavior of crystals can be influenced by altering the state of the surface. This is attributed to the structural changes of the crystal lattice in the surface and subsurface regions and subsequent dislocation behavior in these regions. The effects of an interface are numerous and complicated.[5] It is generally true that the interface can either create a barrier to dislocations generated in the bulk material during plastic deformation or interfere with preferred dislocation multiplication in the surface region. Different strengthening mechanism(s) may operate depending on the individual system. For example, Livesay and Starke[5] found that the critical resolved shear stress for vacuum deposited nickel-on-copper and cobalt-on-copper systems were greatly increased when compared with the pure copper crystal. The results were explained in terms of the image forces due to differences in elastic modulus between the substrate and the coating. The shear modulus of nickel and cobalt are respectively 54 percent and 69 percent higher than that of copper. Under these circumstances, the image force is repulsive to the

dislocations near the surface and thus block dislocation egression.

However, this dominant factor should be applied only to those systems which contain an abrupt interface, small lattice misfit and compatible crystal structures. Otherwise, many other factors should be taken into account. Patterson and Greenfield[6] showed that when the coating material was diffused into the substrate an alloyed interface was created which also caused a strength increase. In their case, however, the effect was attributed to solid solution hardening. Here, the elastic interaction of glide dislocations with solute atoms and a solute concentration gradient were the main contributors. The coherency at the interface can also play an important role. The lattice misfit between the coating film and the substrate will be accommodated by elastic strains in the two lattices and by an array of misfit dislocations. This strain field and the accommodating networks are the dislocation barriers, a fact which has been confirmed experimentally.[7] In addition, dislocations are obstructed when moving from one crystal structure to another, since the Peierls force, Burgers vector, and resolved shear stress are changed.

Kramer[8] has introduced the idea of a surface layer stress and applied it to surface coated systems. He proposes that a region of high dislocation density, the so called "debris layer," is formed near the surface during

plastic deformation. This layer not only impedes the escape of dislocations, but also provides a barrier against which dislocations may pile up. By this means, he suggests that a stress which opposes the motion of dislocations is generated. He and his coworkers[9,10] have used this idea to interpretate various aspects of plastic deformation. For example, the creep rate of fcc single crystals was shown to increase markedly when the specimens were polished during the test.[9] They associated this with the continuous removal of the debris layer. Also, the tensile and creep properties of aluminum were greatly changed in vacuum.[10] The work hardening rate and the activation energy for creep decreased with the lowering of the test pressure. If their concepts are extended to a surface coated system, the mechanical characteristics of the substrate surface layer should be modified by a surface coating, and a change in plastic deformation behavior should be expected.

Surface conditions which have been shown to affect the fatigue life are as follows:

1. Surface roughness. Since early days of fatigue study, it has been recognized that fatigue performance can be appreciably affected by different types of surface finish. Even the very fine scratches left on the surface after machining can act as stress raisers which are detrimental to the fatigue performance of a part. Ground and polished surfaces have been shown to have a fatigue life ten times

better than a machined surface.[11]

2. The state of residual stresses. The formation of the beneficial compressive residual stress on the surface has long been used in industry as a chief method of increasing fatigue performance. The most widely used methods are shot peening and surface rolling. The compressive residual stress on the surface produced by these methods can balance part of the externally applied tensile stress and then decrease the possibility of fatigue crack initiation.

3. The changes in surface properties. There are some indications that fatigue properties will be increased by having a harder and stronger surface.[12] Case carburizing and nitriding are good examples. However, since favorable compressive residual stresses are also created by these processes, it is highly doubtful that this improvement is exclusively due to the higher strengthened surface. Grosskreutz and Benson[13] had only scattered success in increasing the fatigue life by diffusing copper into aluminum to raise the surface yield strength. Other results have also shown that the fatigue life is not always increased by a hard coating. The fatigue life of steel was found to decrease when electroplated with chromium.[14] Of course, the electroplating process may generate some problems which are harmful to fatigue. In strain controlled fatigue a high level of stress must be reached before yielding would occur in a hard coating. This high stress and low tolerance of

plastic flow makes it likely that cracks will begin earlier.

Greenfield and Snyder[15] observed that a small alteration in the surface condition of Ti-6Al-4V had a significant effect on fatigue life. Among all the possible reasons, they concluded that solid solution hardening, twin formation and grain boundary effects seemed to be the major factors; others, such as shear modulus and stacking fault energy changes in the surface area were less important. Kramer[16] approached the same problem from the concept of surface layer stress. He proposed that during cycling, the surface layer stress increases, and when it reaches the fracture strength, a fatigue crack will initiate. During cycling, the crack tip ends at the point where the stress gradient in the surface layer equals the fracture strength. In the following cycle, the crack will propagate further with the increasing surface stress. Based on this assumption, the fatigue endurance limit is the stress amplitude below which a surface layer stress will not form, or the rate of increase of surface layer stress is negligibly small. The change of fatigue life due to a surface coating would then depend on how it changes the surface layer stress.

Microscopically, a typical fatigue failure consists of two stages: crack initiation and crack propagation.[17] Cracks always initiate at the surface unless there exists some internal defects. As for surface coated materials, once a crack initiates on the surface and penetrates through

the coating layer into the bulk material, the propagation process is the same as for the uncoated material. Therefore, the change of fatigue behavior due to surface coating is mainly associated with the crack initiation stage.

For a pure single phase material, fatigue crack initiation sites normally are slip bands, grain boundaries and twin boundaries. Slip band studies have been given the most attention. As early as 1903, Ewing and Humphrey[18] observed slip bands in some grains within the first few thousand cycles when they fatigued wrought iron samples by rotational bending, even at stress amplitudes below the macroscopic yield point. Continued cycling only added a few more slip bands to the previous ones, however the slip bands became more intense and were finally the initiation sites of fine cracks. Unfortunately, in the next fifty years, very little fundamental work was done. Most fatigue work was devoted to the determination of the fatigue life. However, in recent years, after the development of transmission electron microscopy and x-ray techniques, the metallography of fatigue has been widely studied.

Forsyth[19] discovered the slip band extrusion effect, while other workers[20] found the slip band intrusion effect. Thompson et al.[21] electropolished fatigued copper samples to remove the slip bands and extend the fatigue life enormously. Alden and Backofen[22] found that the slip band formation and crack initiation was completely prevented by a thick anodic

film on the surface.

As slip band crack initiation was gradually accepted, its basic characteristics became known. Wood[23] and many others[24,25] examined the tapered section of the fatigued specimen and identified the notch-peak topography of the slip bands on the surface. These notches were stress-raisers which ensured the continuity of the localized strain. In addition, the slip band was found to be softer than the matrix.[26] That means they have lower flow stress and work hardening rate, both of which favors their continued local development. Woods[27] observed, in agreement with other workers,[28] that the slip bands in copper were gathered together in thick bands where all plastic strain was localized as the fatigue process continued. Actually, the fraction of the gauge length covered with these slip bands as fatigue reached saturation seemed to have a linear relationship with the applied plastic strain amplitude.[28,29] This implies that cyclic strain in a fatigued single crystal is controlled primarily by repeated slip within the persistent slip band.

The microstructure of slip bands formed during fatigue in copper specimens consist of dislocation cell structure regardless of the strain amplitude.[25,30] The same structure appears in bulk material only when the strain amplitude is high.[31] However, recent results by Finney and Laird[28] suggest that this is not so. They believe that, at least for copper single crystal oriented for single slip, slip

bands consist of parallel walls of dislocations and a cell structure develops only after these walls fill the whole specimen. In other words, cell structures are not formed until the strain amplitude reaches a certain level whereby the wall structure can no longer accommodate the imposed strain. They also believe that persistent slip bands penetrate throughout the whole thickness of the specimen, but no direct evidence was demonstrated. This conflicts with early conclusions that slip bands are first initiated on the surface and grow inwardly.[25,30] These results were based on observations that the cell structure of the slip bands decreased in intensity in regions deeper into the specimen and finally completely disappeared.

Slip band crack initiation in fatigue is due to the characteristics of its notch-peak topography. This is a result of the localized strain and irreversible slip associated with the slip band. Therefore, homogeneous and reversible slip systems should retard crack initiation. This can be accomplished by having a system with a more planar slip mode.

In the past decade, many workers[32,33,34] have succeeded in this respect by lowering the stacking fault energy of the material. Lowering the stacking fault energy inhibits the incidence of easy cross-slip, and promotes the planar slip mode. McGrath and Thurston[32] worked on copper-zinc alloys and found that the coarse slip bands became

narrower as the concentration of zinc increased and the stacking fault energy decreased. Avery and Backofen[33] systematically lowered the stacking fault energy of copper-aluminum system below 20 ergs/cm$^2$ and found no slip band appeared on the surface fatigued in plane bending with a total strain amplitude of 0.2 percent. Moreover, in both of these cases, there were indications that not only the crack initiation had been delayed, but the crack propagation rate was also reduced. The inhibition of cross-slip restricted the spread of the plasticity at the crack tip.[35] If fatigue crack growth is governed by a blunting mechanism,[36] however, the crack propagation rate should be decreased with increasing incidence of cross slip.

The present study was designed to investigate how the low cycle fatigue behavior is affected by altering the surface conditions by ion plating materials of various SFE's.

# CHAPTER III

# EXPERIMENTAL TECHNIQUES AND PROCEDURES

## Ion Plating

Ion plating process is a newly developed vacuum coating technique. The sample is first cleaned in a vacuum chamber by sputtering. This is accomplished by introducing an inert gas, such as argon, into the chamber and then applying a potential difference (1-6 kilovolts) between a vaporizing filament and the sample, with the sample at the lower potential. The field has no significant effect on the neutral atoms of the gas, but those few which are ionized are accelerated in the direction of the electric field while the liberated electrons are accelerated in the opposite direction. The energy gain of these particles is on the order of thousands of electron volts while the ionization energy of the atoms is on the order of a few electron volts; thus the energetic particles cause further ionization. This chain reaction produces a number of gas ions which impinge on the sample surface with sufficient energy to eject surface atoms (sputtering) and electrons, thus cleaning the surface and also adding electrons to the gas. The sputtering is done dynamically via an equilibrium gas bleed so that the sputtered atoms are swept out of the system and the sample

surface cleaned. After the surface is cleaned, but while the sputtering is continuing, the plating material is vaporized as in vapor deposition. The vaporized plating atoms then experience the effect of the electric field in the same way as the gas atoms did, being ionized and striking the surface with high energy. Since the sputtering gas is still available, the film is the result of plating plus sputtering.

The film produced is different from that in vapor deposition in a number of ways. Since the plating atoms strike the surface with significant energy, they will travel some distance into the material before coming to rest. This produces a film of unusually good adherence. In addition, since the ions are accelerated in the direction of the field, they will uniformly cover a sample whose geometry is relatively smooth. For complex geometries the film is not completely uniform because of the inertia of the ions in the distorted field, however, it is much more so than for vapor deposited films. These two properties make the ion plating an attractive coating process. There is a third large difference between ion plating and vapor deposition and this is the character of the interface formed. The penetration of the atoms during vapor deposition is extremely small since they possess only thermal energy, thus the interface is quite sharp. In ion plating the penetration is comparatively large with the result that there is a gradual interface which consists of a zone of substrate, sputtering and plating atoms.

There are many factors that determine the characteristics of ion plated coatings. The penetration depth and the thickness of the coating material depends on the potential across the electrodes, the filament current, pressure inside the chamber, temperature and the evaporation time. Up to now, there is still no monitoring device which can accurately control the coating thickness. The absolute value of the coating thickness in the present study was not a critical variable. The main concern was the uniformity across the gauge section of the test sample and the same film thickness on all the specimens within a group. Since an exact duplication of ion plating was impossible, this goal was accomplished by ion plating the whole group of specimens at the same time. A precise weight measurement (to $10^{-4}$g) method was used to calculate the coating thickness. Weight loss of a crystal sputtered in argon plasma was first measured under different conditions. The net weight charge due to ion plating was assumed to be the combination of the weight gain from the coating material and the weight loss due to sputtering. The coating thickness was calculated from the measured weight change and the surface area of the specimen. The ion plating apparatus used is shown in Figure 1. The procedure of ion plating followed in this study is:

1. Mount the filament (a 6 inch circular tungsten wire) and the samples on the cathode (a circular copper plate).

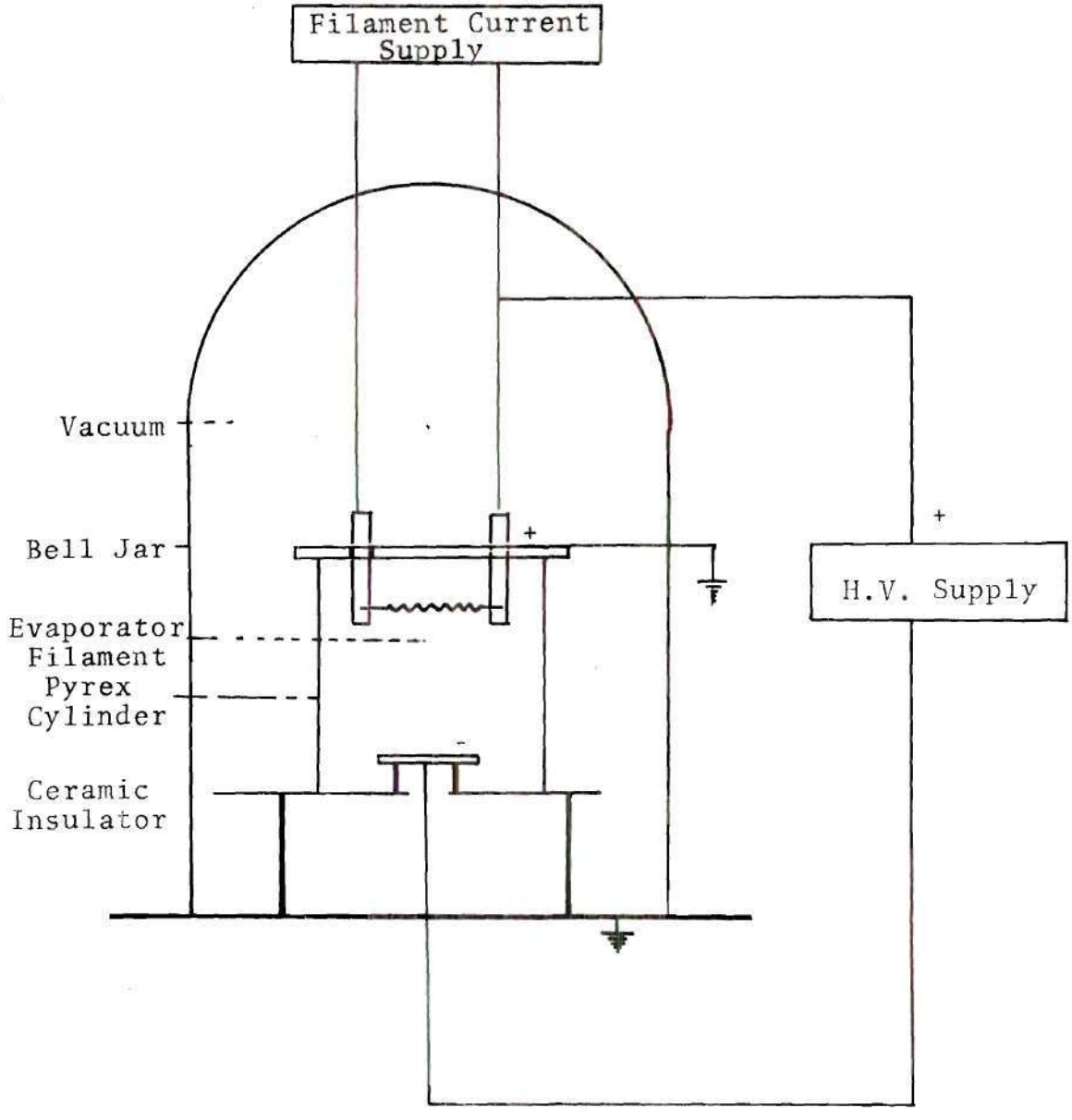


Figure 1. Ion-Plating Apparatus Used in this Study

2. Pump down the system inside the bell jar until the pressure is below $10^{-5}$ torr.

3. Let in a small amount of argon gas through a variable leak valve and then evacuate the system. Repeat the same process several times.

4. Maintain the pressure inside the chamber at about 20-25 μm by balancing the inflow argon rate and pumping rate.

5. Apply the voltage across the electrodes gradually to 2.5 kv or 3.5 kv until a pinkish-violet plasma is formed.

6. Maintain sputtering for about 5 minutes. In the meantime, the cathode current will drop to a stable value.

7. Turn on the filament power supply. Increase the filament current very slowly until the coating material is melted and wets the filament.

8. Keep evaporating for about 20 seconds.

9. Shut off the high voltage power supply first, then reduce the filament current to zero.

10. Evacuate the system. Wait until the system is cooled and remove the samples.

Following this procedure the coating thickness of the silver plated specimens were approximate 2 μm, the copper plated ones were 2.5 μm, "thin" nickel plated specimens were 1 μm, "thick" nickel plated specimens were 2.5 μm. These values were checked by direct measurement from the highly magnified scanning electron micrographs of the sectioned

specimen. They were in quite good agreement with the values calculated by weight change.

## Growth of Single Crystal

Single crystals with circular cross section (4 mm diameter) were grown from 99.999 percent copper in a split graphite mold by using the Bridgman method. To ensure the uniformity of crystal orientation for all crystals, seeded crystals were used. The orientation of all crystals, which is shown in Figure 2, was verified by back reflection Laue patterns.

## Sample Preparation

The specimens used in this work were cylindrical. Actually, for surface topographic studies, flat specimens would have been more desirable. However, this research was mainly concerned with fatigue life studies, and edged specimens will create the inevitable stress concentration at the corners and consequently alter the fatigue crack initiation and propagation behavior. In addition, for complex geometries, the ion plated film is not uniform because of the edging effect, since the ions are accelerated in the direction of the electric field, and the field is distorted due to the geometric irregularities.

Fatigue and tensile specimens were prepared from the single crystals by spark machining. The final gage lengths for fatigue samples were 3 mm diameter by 6 mm long, while

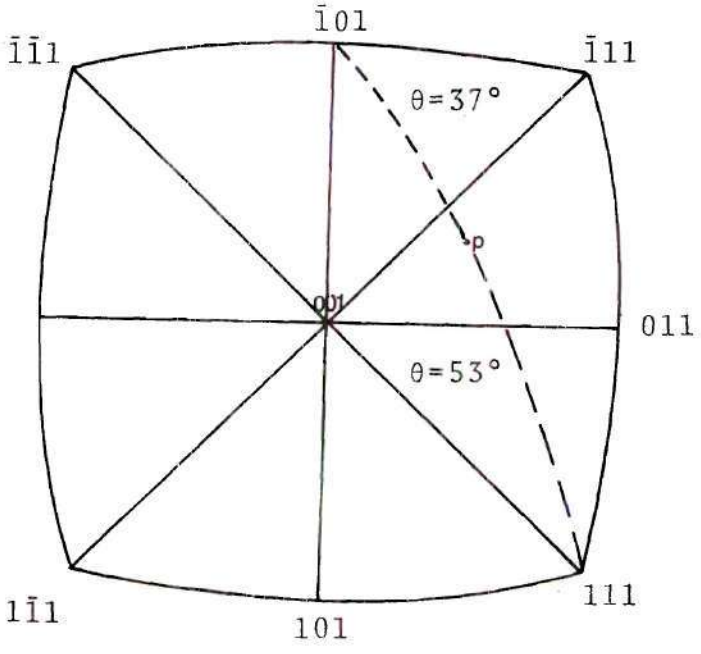


primary slip system (111) ($\bar{1}01$)

cross-slip plane ($1\bar{1}1$)

conjugate plane ($\bar{1}\bar{1}1$)

critical plane ($\bar{1}11$)

Figure 2. Orientation of the Crystals Used in this Study

the tensile samples were 3 mm diameter by 12 mm long. Immediately after each sample was machined, it was cleaned in diluted nitric acid, replaced in a graphite mold and encapsuled in Vycor under a vacuum of $10^{-5}$ torr. They were then annealed at 950°C for 4 hours and furnace cooled. Finally, the specimens were electropolished at room temperature in 70 percent orthophospheric acid and 30 percent distilled water and then ion plated. For copper plated and silver plated samples, the applied voltage was 2.5 kv. For nickel plated samples, both 2.5 kv and 3.5 kv were used for two different groups. The thickness of the coatings were of the order of a few microns as mentioned earlier.

## Surface Residual Strain Determination

Some flat copper single crystals were sputtered and ion plated at different potentials. The residual strain resulted from the different sputtering conditions was determined by the Warren-Averbach[37] x-ray line broading technique. Four samples were sliced from a flat copper single crystal. After the surface was electropolished, the samples were vacuum annealed at 950°C for 100 hours. Then one of them was sputtered in argon plasma for 5 mintues. The other two were ion plated with nickel at 2.5 kv and 3.5 kv respectively.

The intensity distribution was measured for the (111) and (222) reflections by automatic step scanning in 0.02° 2θ increments using a Cu target tube. The time for intensity

accumulation was 24.5 seconds and the 2θ range covered was ±2° about the maximum intensity point. The intensity profiles were transformed into a Fourier series using computer technique described elsewhere. The Rachinger method[38] was applied for correction of the $\alpha_1\alpha_2$ doublet and data from a fully annealed copper sample was used for the instrumental correction employing the method of Stokes.[39] The corrected Fourier coefficients, A (L), were used to calculate the root-mean-square strain.

The root mean square strain $(\overline{\varepsilon_L^2})^{1/2}$ was calculated from the equation:

$$(\overline{\varepsilon_L^2})^{1/2} = \frac{d[\ell n\ A_L^S - \ell n\ A_L\ (\frac{1}{d})]^{1/2}}{\sqrt{2}\ \pi\ L}$$

where

d is the interplanar spacing of a particular (hkl)

L is the real distance perpendicular to the diffraction plane.

In order to find the value of $A_L^S$, at least two orders of reflection are required for the Fourier-analysis. For a fixed value of L, the intercept of the plot the value of $A_L(\frac{1}{d})$ vs $\frac{1}{d^2}$ at $\frac{1}{d^2} = 0$ is the value of $A_L^S$.

Low Cycle Fatigue Test

The low cycle fatigue tests were performed on an

Instron testing machine (model TT-DM-L). The load range used was ±100 kg if the strain amplitude was ±1 percent, otherwide, it was ±250 kg. The samples were fatigued at room temperature in air with constant total strain amplitude ranging from ±1 percent to ±5 percent. The strain was measured with a 10 mm Instron extensometer clamped to stands rigidly fixed to the grip. A self aligning Woods' metal reservoir was used to insure the coincidence of the machine axis with the specimen axis. The strain rate was $3 \times 10^{-3}$ $sec^{-1}$ which was equivalent to a cyclic frequency of 1 to 4 cycles per minute depending on the strain amplitude used. The load-extension curves were automatically plotted on the chart and peak loads were manually recorded for fatigue hardening/softening analysis. Some tests were carried to fracture and some were stopped prior to fracture for slip line and TEM examination.

## Microscopic Studies on Fatigue Samples

Three sets of pure copper, nickel plated and silver plated samples were examined. Three samples in each set were removed from the grips after being fatigued at ±1 percent of total strain amplitude for 30, 300 and 1200 cycles respectively and the slip bands were examined by scanning electron microscopy. Qualitatively, the heights of these bands were compared by interferometry studies using a Michelson interferometer[40] and a mercury vapor lamp as the

light source.

After the surface studies, the specimens were prepared for transmission electron microscopy studies. Sections were cut parallel to primary and conjugate slip planes from the gauge length by spark cutting. The sections were then chemically thinned, dimpled by an electrolytic jet, electropolished until perforation, and examined in a Siemens electron microscope.

# CHAPTER IV

# RESULTS

## Unidirectional Tensile Test

Figure 3 shows the stress-strain curve obtained for pure copper, nickel plated, and silver plated, copper single crystals. All curves display clearly the three stages of work hardening: I. easy glide, II. rapid work hardening, III. dynamic recovery. The critical resolved shear stress increased from 35 $g/mm^2$ for pure copper to 56 $g/mm^2$ by nickel plating, while it decreased to 29 $g/mm^2$ by silver plating. Copper plated crystals virtually showed no change when compared to unplated crystals. The extent of the stage I deformation was generally shortened by all surface coatings. When the deformation was well into stage III, the curve of the nickel plated crystal was above those of pure copper and the silver plated crystals. During the unidirectional deformation, the ion-plated coating film and the substrate deformed as a continuum. No peeling or scaling effect was observed, even when pulled to fracture.

## Surface Residual Strain

The diffracted line profile of the sputtered specimen did not show any distinguishable broadening effect when compared with that of a fully annealed sample. One may

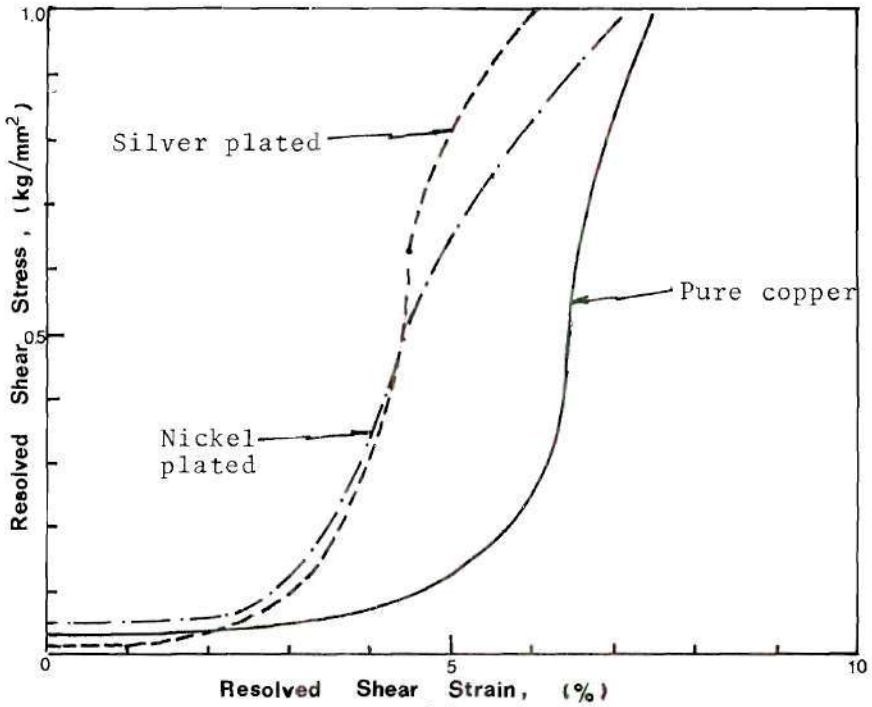


(a)

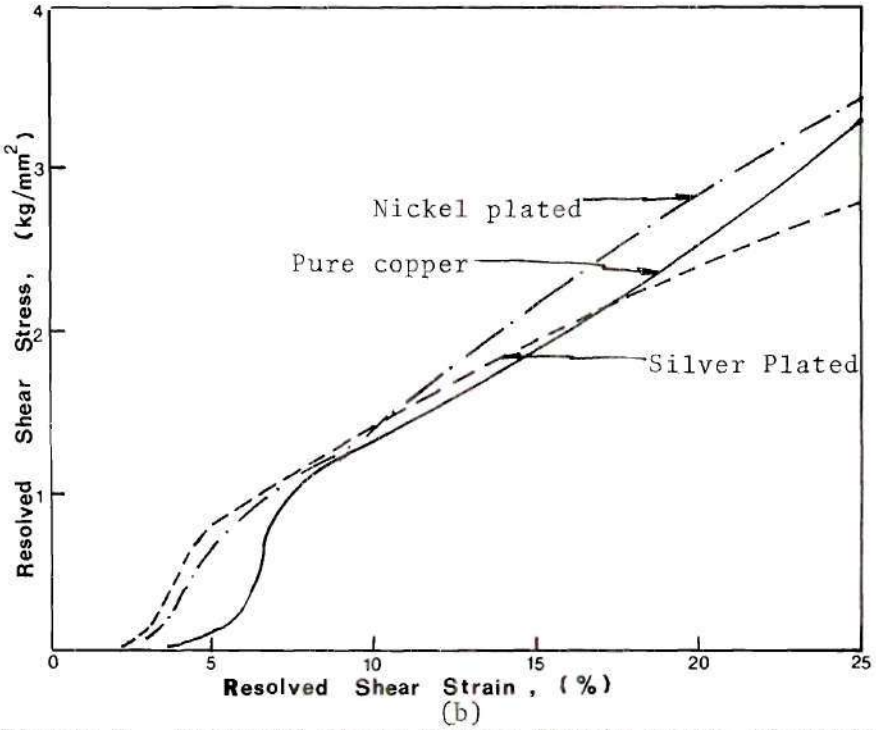


(b)

Figure 3. Resolved Shear Stress-Strain Curve of Unidirectional Test (a) At very early stage, (b) Deformed into Stage III

conclude that the residual strain due to the sputtering process of the present study was quite small; as evidenced by the root-mean-square strain, $\overline{(\varepsilon_L^2)}^{1/2}$, evaluated from the (111) and (222) peaks of a copper single crystal, of $10^{-4}$, Table 1. However, the accelerating voltage across the electrodes did influence this value, as expected.

## Fatigue Hardening and Softening

Figures 4 through 7 show the cyclic behavior of the different sets of specimens tested over a range of strain amplitudes. The curves are plots of the mean peak shear stress amplitude versus the corresponding number of cycles. The mean peak stress amplitude, defined in this study, is the average value of the peak tensile and compressive stress in each cycle. The compressive peak load was always greater than the tensile peak load, especially in the early period of cycling. This difference increased with increasing strain amplitude. The shear stress was resolved on the primary slip system, since the surface trace study revealed that slip occurred predominantly on this system.

Since all crystals were initially annealed, cyclic strain hardening was first observed. During the first 20 to 40 cycles, the cyclic hardening increased rapidly, but the hardening rate decreased until it approached zero. Both the cyclic hardening rate and the saturated stress amplitude increased with increasing strain amplitude. Saturation was

Table 1. Observed Root-Mean-Square Strain

| Sample | Applied Voltage | L | $(\overline{\varepsilon_L^2})^{1/2}$ |
|---|---|---|---|
| Cu Ar bombarded | 2.5 kv | 50 Å | 0.084% |
| | | 100 Å | 0.032% |
| Ni plated on Cu | 2.5 kv | 50 Å | 0.077% |
| | | 100 Å | 0.0295% |
| Ni plated on Cu | 3.5 kv | 50 Å | 0.153% |
| | | 100 Å | 0.086% |

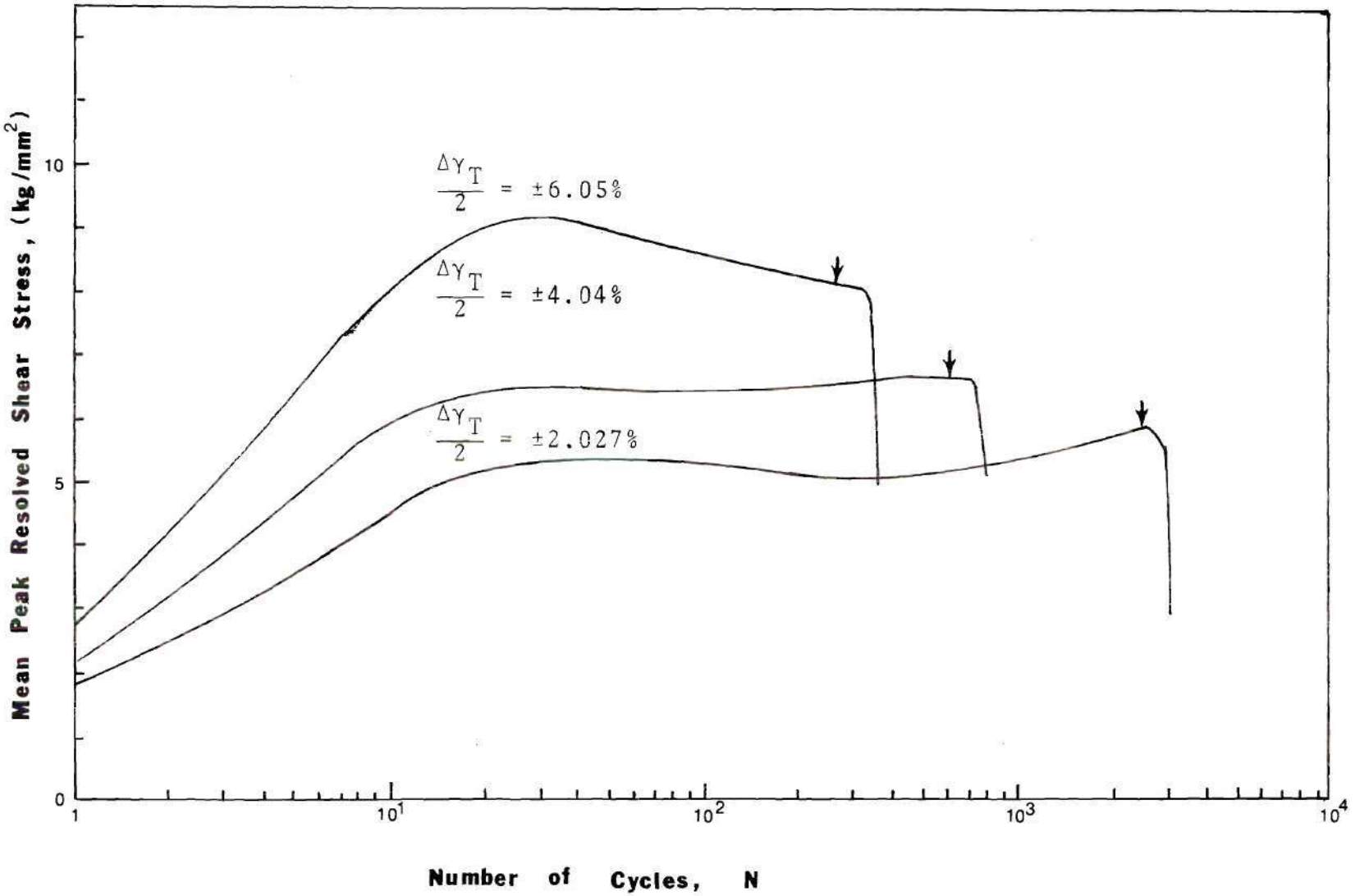


Figure 4. Cyclic Hardening/Softening of Pure Copper at Room Temperature and Various Amplitudes

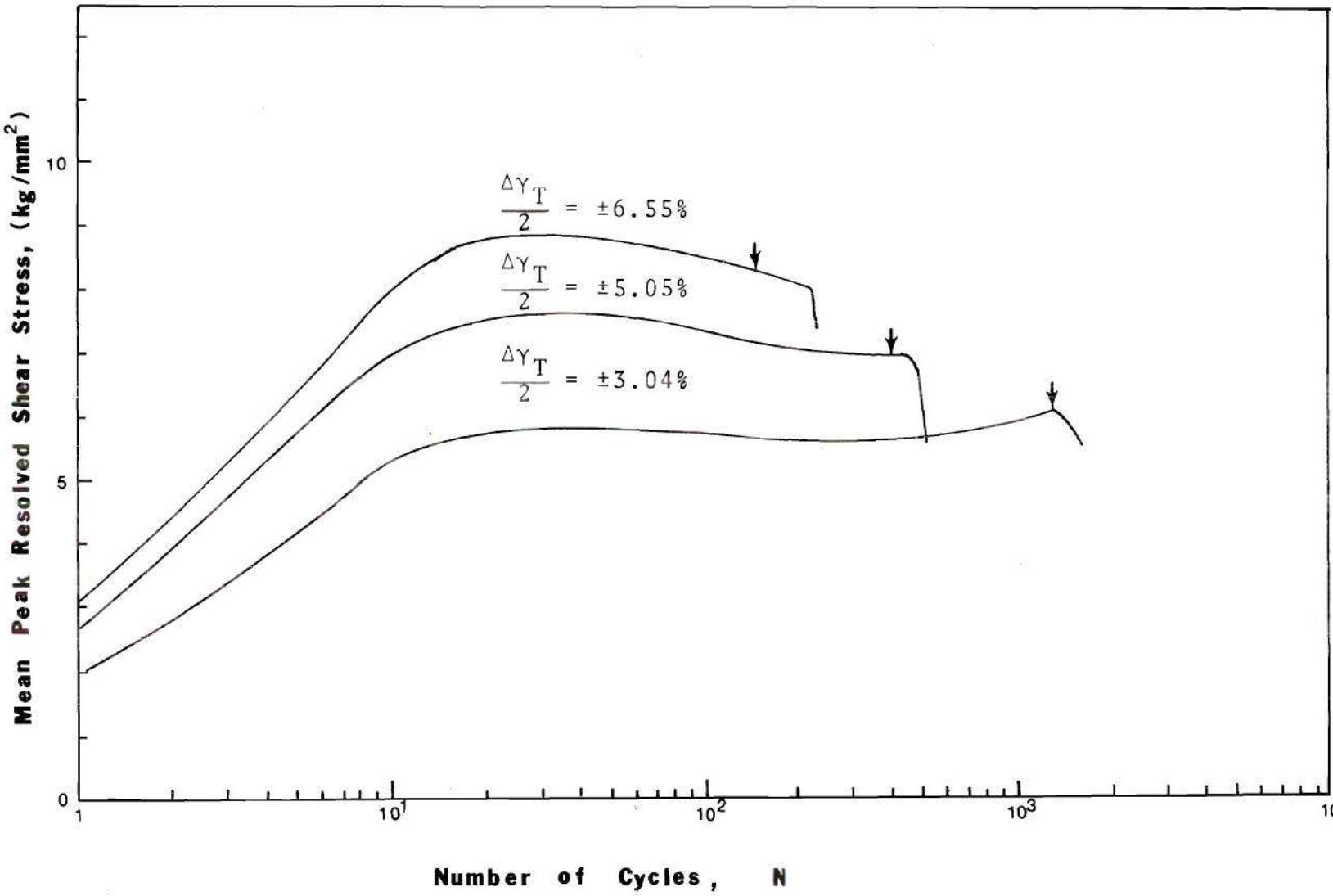


Figure 5. Cyclic Hardening/Softening of Copper-Plated Copper at Room Temperature and Various Amplitudes

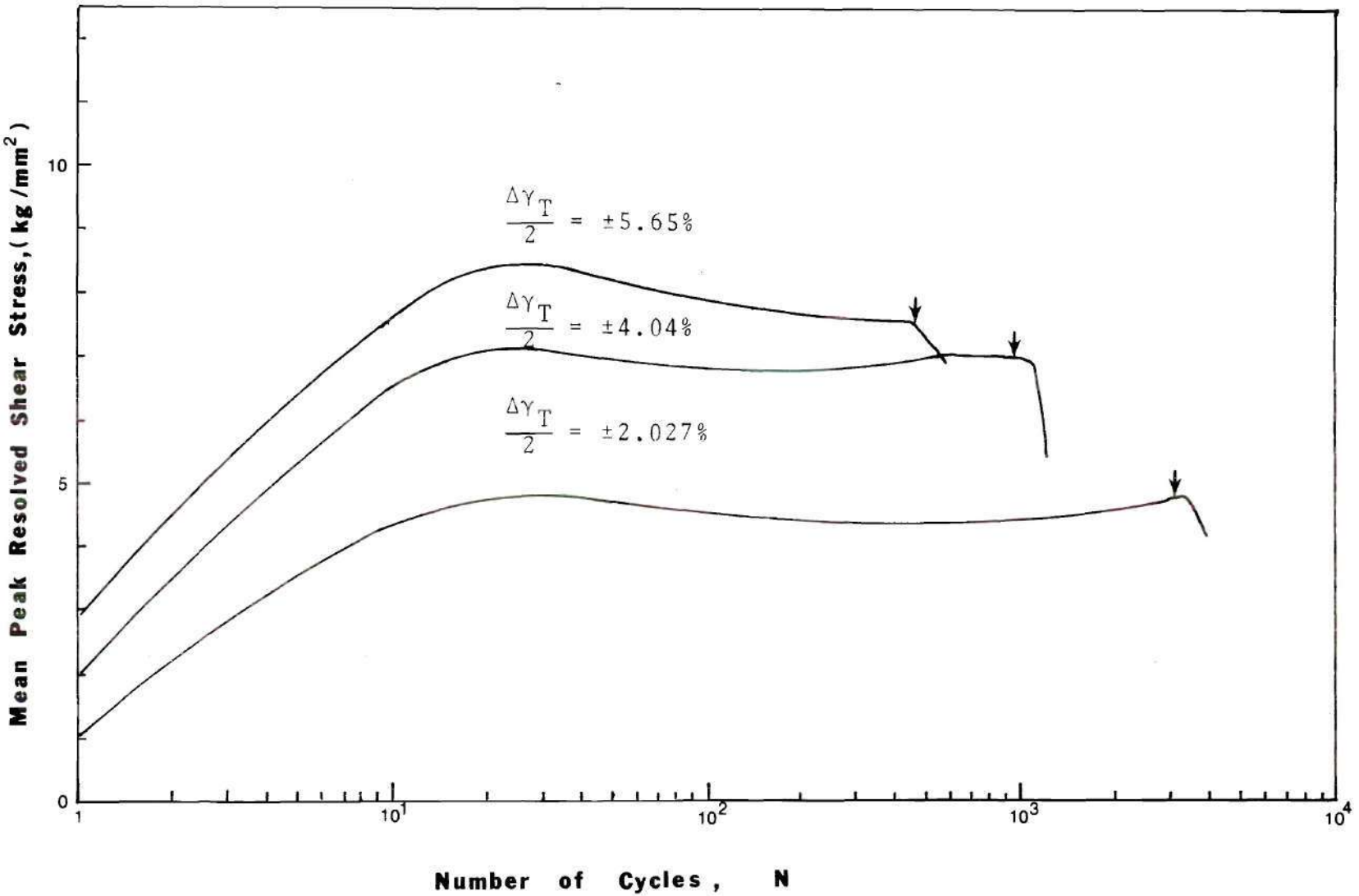


Figure 6. Cyclic Hardening/Softening of Silver-Plated Copper at Room Temperature and Various Amplitudes

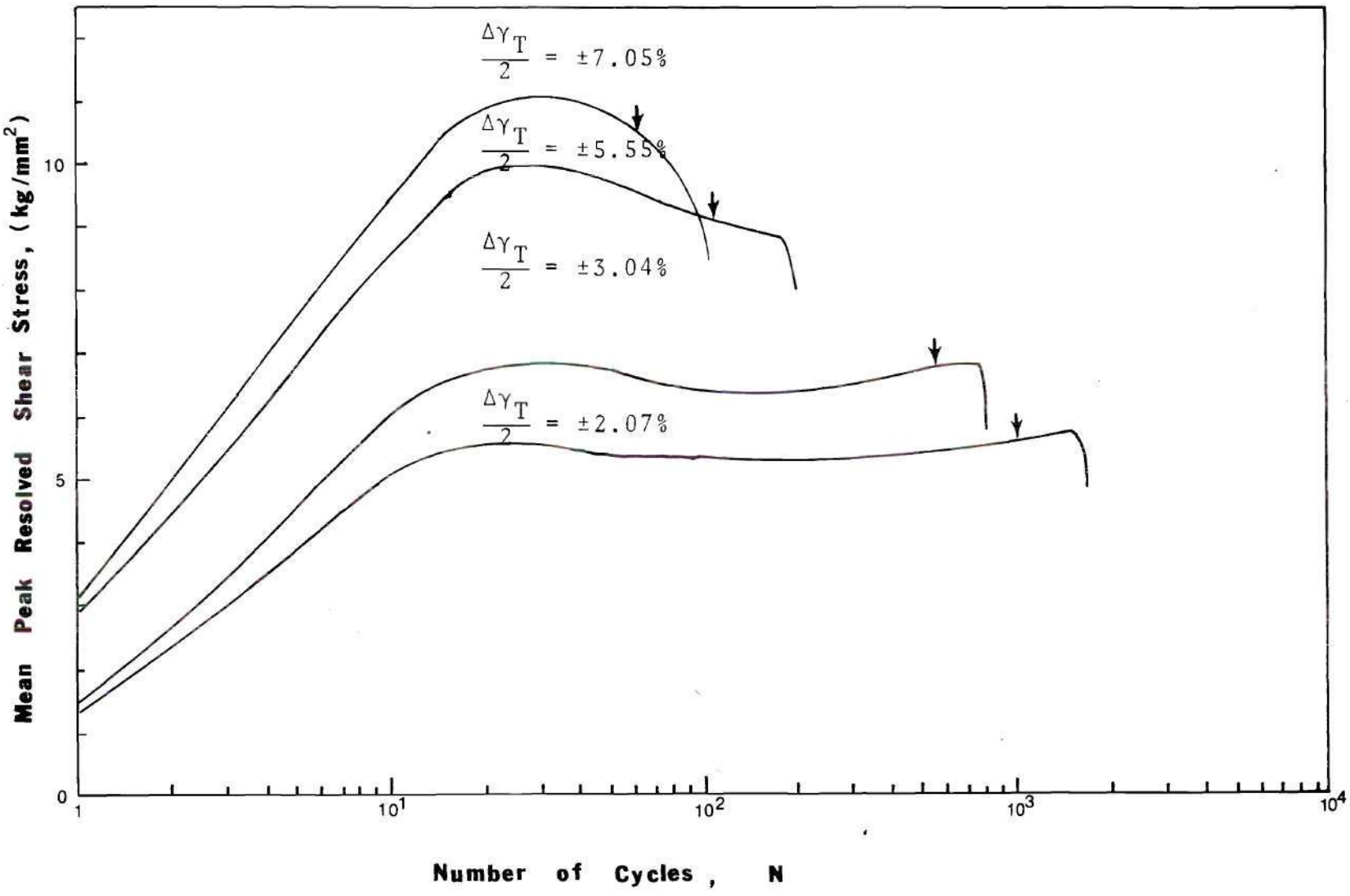


Figure 7. Cyclic Hardening/Softening of Thick Nickel-Plated Copper at Room Temperature and Various Amplitudes

not, however, maintained to fracture; but was followed by cyclic softening. The softening rate was much lower than the initial hardening rate and successive peak stress amplitudes were only slightly decreased. For pure copper crystals cycled at ±1 percent total strain amplitude ($\frac{\Delta\varepsilon_T}{2}$), the fatigue softening lasted for about 350 cycles. The corresponding peak shear stress amplitude dropped from 5.44 $kg/mm^2$ at the initially saturated state to a minimum of 5.1 $kg/mm^2$ in the fatigue softening region.

Following the cyclic softening stage, there appeared another fatigue hardening stage. The hardening rate in this secondary hardening stage was also small. This stage was terminated when the crack initiated and propagated to a size at which the specimen could no longer sustain the applied load. This always occurred after the crack was observed by the naked eye and is indicated by an arrow on the curve. Hysteresis loops of the pure copper crystal fatigued at $\frac{\Delta\varepsilon_T}{2}$ = ±1 percent are shown in Figure 8. These curves represent the changes of the peak load and the dissipated energy per cycle for the initially saturated fatigue softening and the secondary fatigue hardening stages. For very high strain amplitudes ($\frac{\Delta\varepsilon_T}{2}$ > ±2 percent), only rapid fatigue hardening, saturation and fatigue softening was observed. This was due to early crack formation.

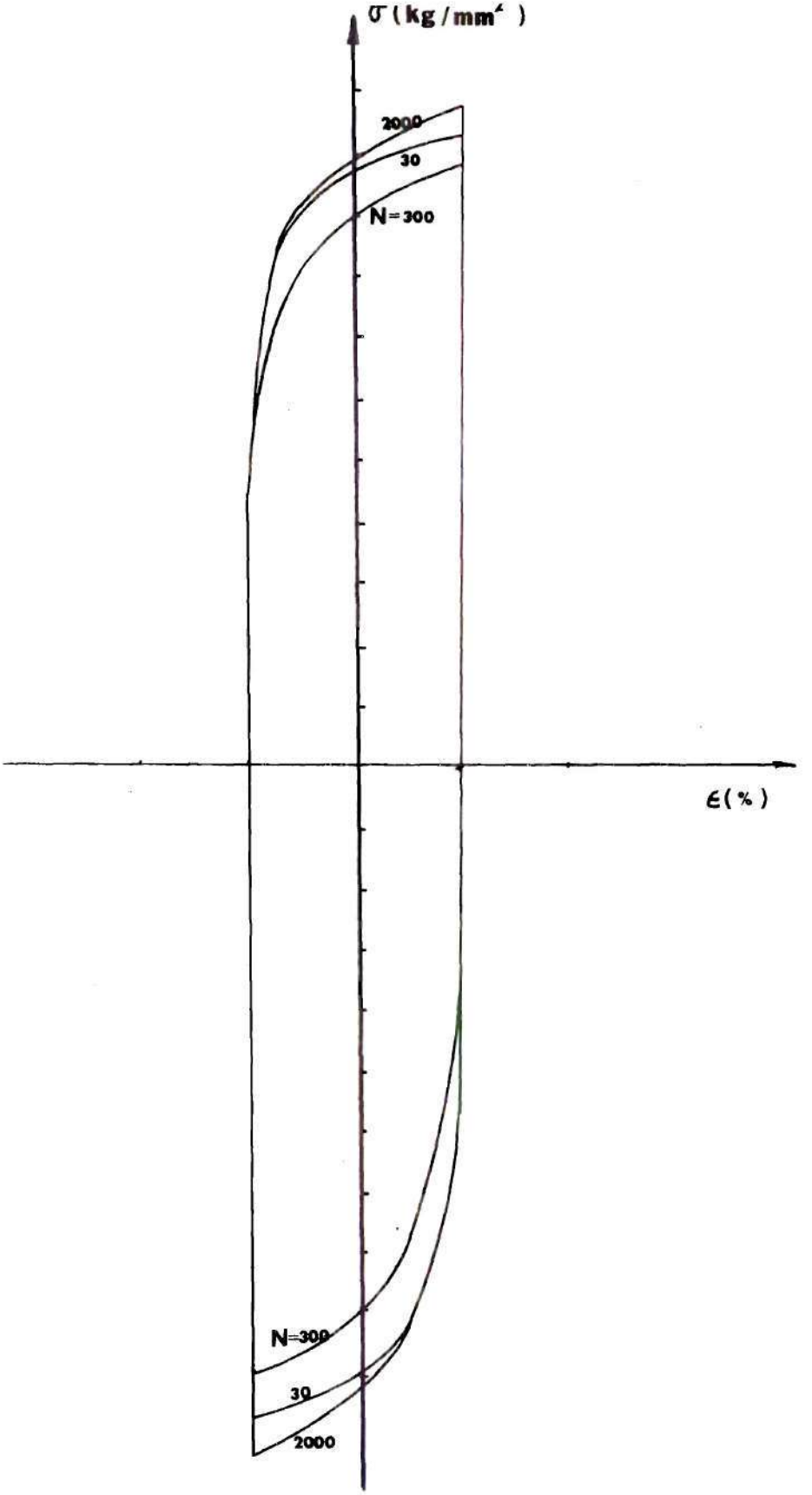


Figure 8. Hysteresis Loops for Pure Copper Crystal Fatigued at $\frac{\Delta\varepsilon_T}{2}$ = ±1 Percent at Different Stages of Cycling

## Low Cycle Fatigue Behavior

The test results of the ion plated specimens and the uncoated specimens are summarized in Table 2. The plots of the plastic strain amplitude versus the number of reversals to failure are shown in Figure 9. The plastic strain amplitude is represented by the half width of the hysteresis loop at zero load when the crystal reached its initially saturated state. Actually, this value changed only slightly with further cycling.

A series of tests were first conducted on the uncoated specimens. The data could be represented by the Manson-Coffin low cycle fatigue law, which states that the plastic strain amplitude ($\frac{\Delta\varepsilon_p}{2}$) has a linear relationship with the number of cycles to failure ($N_f$) on a log-log scale:

$$\frac{\Delta\varepsilon_p}{2} = \varepsilon_f' \, (2N_f)^c$$

where $\varepsilon_f'$ is the cyclic strain coefficient, c is the fatigue ductility exponent. Therefore, the Manson-Coffin low cycle fatigue law for uncoated copper crystals can be written as

$$\frac{\Delta\varepsilon_p}{2} = 0.55 \, (2N_f)^{-0.445}$$

This curve was used as a basis for comparison with ion-plated specimens.

Table 2. Low Cycle Fatigue Data of Uncoated and Coated Copper Crystals

| Specimen | Frequency cpm | Total Strain Amplitude $\frac{\Delta\varepsilon_t}{2}$ % | Total Shear Strain Amplitude $\frac{\Delta\tau_t}{2}$ % | Cyclic Stress-Strain Data at $\frac{\Delta\sigma}{\Delta N} = 0$ | | | | | | | | | |
|---|---|---|---|---|---|---|---|---|---|---|---|---|---|
| | | | | Stress Amplitude $\frac{\Delta\sigma}{2}$ $\frac{kg}{mm^2}$ | Shear Stress Amplitude $\frac{\Delta\tau}{2}$ $\frac{kg}{mm^2}$ | Plastic Strain Amplitude $\frac{\Delta\varepsilon_p}{2}$ % | Plastic Shear Strain Amp. $\frac{\Delta\gamma_p}{2}$ % | Elastic Strain Amplitude $\frac{\Delta\varepsilon_E}{2}$ % | Elastic Shear Strain Amp. | No | $N_f$ | $N_p = N_f - N_o$ | $No/N_f$ |
| A1 | 4.2 | 1.00 | 2.03 | 11 | 5.44 | 1.0 | 2.03 | 0 | 0 | 2470 | 3241 | 771 | 0.80 |
| A2 | 2.1 | 2.00 | 4.04 | 13.2 | 6.53 | 1.85 | 3.74 | 0.15 | 0.3 | 625 | 816 | 191 | 0.76 |
| A3 | 1.4 | 3.00 | 6.05 | 18.4 | 9.11 | 2.74 | 5.53 | 0.26 | 0.52 | 265 | 356 | 91 | 0.74 |
| A4 | 1 | 4.00 | 8.05 | 20.9 | 10.09 | 3.65 | 7.35 | 0.35 | 0.80 | 97 | 183 | 86 | 0.53 |
| B1 | 2.8 | 1.50 | 3.04 | 11.8 | 5.84 | 1.45 | 2.94 | 0.05 | 0.1 | 1300 | 1769 | 469 | 0.74 |
| B2 | 1.7 | 2.50 | 5.05 | 15.4 | 7.7 | 2.29 | 4.63 | 0.21 | 0.42 | 400 | 534 | 134 | 0.75 |
| B3 | 1.3 | 3.25 | 6.55 | 17.7 | 8.85 | 2.9 | 5.85 | 0.35 | 0.70 | 145 | 238 | 93 | 0.61 |
| C1 | 4.2 | 1.00 | 2.07 | 9.6 | 4.76 | 1.0 | 2.03 | 0 | 0 | 3200 | 4161 | 961 | 0.77 |
| C2 | 2.1 | 2.00 | 4.04 | 14.4 | 7.17 | 1.82 | 3.68 | 0.18 | 0.36 | 950 | 1190 | 240 | 0.80 |
| C3 | 1.5 | 2.80 | 5.65 | 16.9 | 8.45 | 2.48 | 5.01 | 0.32 | 0.54 | 475 | 599 | 124 | 0.79 |

A = Pure Cu Crystals  B = Cu Plated Crystals

C = Ag Plated Crystals

Table 2 (concluded)

| Specimen | Frequency cpm | Total Strain Amplitude $\frac{\Delta\varepsilon_t}{2}$ % | Total Shear Strain Amplitude $\frac{\Delta\tau_t}{2}$ % | Cyclic Stress-Strain Data at $\frac{\Delta\sigma}{\Delta N} = 0$ | | | | | | No | $N_f$ | $N_p = N_f - N_o$ | $No/N_f$ |
|---|---|---|---|---|---|---|---|---|---|---|---|---|---|
| | | | | Stress Amplitude $\frac{\Delta\sigma}{2}$ $\frac{kg}{mm^2}$ | Shear Stress Amplitude $\frac{\Delta\tau}{2}$ $\frac{kg}{mm^2}$ | Plastic Strain Amplitude $\frac{\Delta\varepsilon_p}{2}$ % | Plastic Shear Strain Amp. $\frac{\Delta\gamma_p}{2}$ % | Elastic Strain Amplitude $\frac{\Delta\varepsilon_E}{2}$ % | Elastic Shear Strain Amp. | | | | |
| D1 | 4.2 | 1.00 | 2.03 | 11.3 | 5.59 | 1 | 2.03 | 0 | 0 | 1000 | 1707 | 707 | 0.59 |
| D2 | 2.8 | 1.50 | 3.04 | 14 | 6.94 | 1.46 | 2.96 | 0.04 | 0.08 | 550 | 794 | 244 | 0.69 |
| D3 | 1.5 | 2.75 | 5.55 | 20 | 9.98 | 2.61 | 5.27 | 0.14 | 0.28 | 107 | 201 | 94 | 0.53 |
| D4 | 1.2 | 3.50 | 7.05 | 221 | 11.07 | 3.22 | 6.49 | 0.28 | 0.56 | 62 | 104 | 42 | 0.60 |
| E1 | 4.2 | 1.00 | 2.03 | 12.2 | 6.06 | 1.00 | 2.03 | 0 | 0 | 1200 | 1935 | 735 | 0.62 |
| E2 | 2.1 | 2.00 | 4.04 | 16.6 | 8.24 | 1.94 | 3.91 | 0.06 | 0.13 | 280 | 442 | 162 | 0.63 |
| E3 | 1 | 4.00 | 8.05 | 22.03 | 11.06 | 3.68 | 7.4 | 0.32 | 0.65 | 35 | 101 | 66 | 0.35 |

D = Thick Ni plated Crystals

E = Thin Ni Plated Crystals

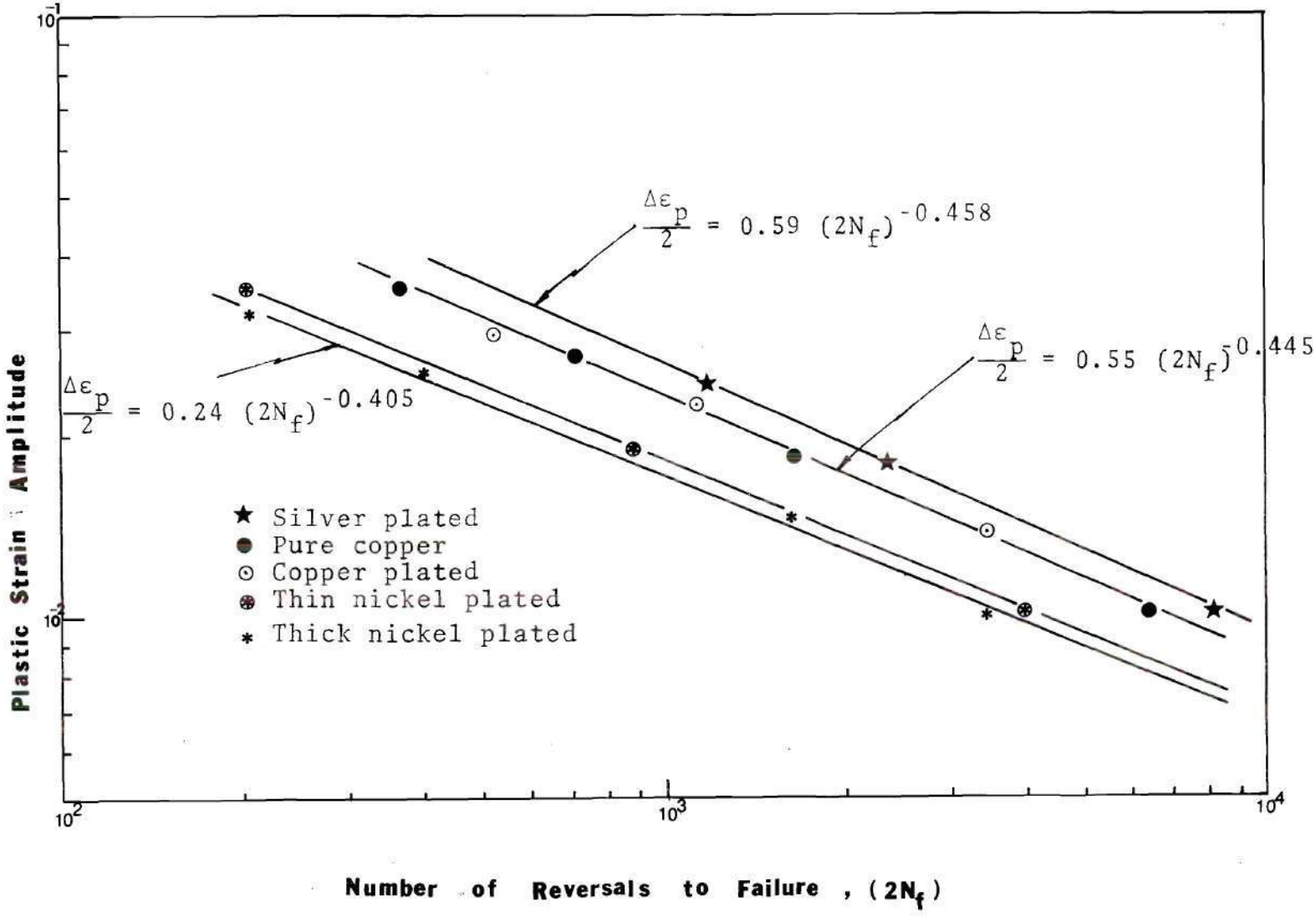


Figure 9. Plastic Strain-Life Curves Showing the Influence of Different Coating Conditions

For copper coated specimens, the controlling strain amplitudes were different from those applied on pure copper crystals. The data points, however, coincided with the curve of the uncoated specimens. It was concluded that copper plating had no significant effect on the low cycle fatigue life of copper single crystals (it also had no effect on the monotonic properties).

For silver plated specimens, it was apparent that the fatigue lives increased. The increase of fatigue lives was mostly due to the retardation of crack formation. Compare the silver plated and pure copper crystals both cycled at $\frac{\Delta\varepsilon_T}{2} = \pm 1$ percent. It took 3200 cycles for the silver plated specimen to create a crack which could be observed by the naked eye, while it took only 2470 cycles for a pure copper specimen. The difference of 730 cycles is 80 percent of the total fatigue life change. The plastic strain amplitude and the fatigue life can be described by

$$\frac{\Delta\varepsilon_p}{2} = 0.59\ (2N_f)^{-0.458}$$

The two groups of nickel plated specimens showed a decrease in fatigue life when compared to the uncoated specimens. An increase in coating thickness was even more detrimental to fatigue life. For the same strain amplitudes, nickel plated specimens had cracks initiated on the surface

much earlier than did the pure copper and the silver plated specimens. Earlier fatigue crack initiation was the main reason for the decrease of total fatigue life. Again the Manson-Coffin's law was obeyed and can be expressed as:

$$\frac{\Delta\varepsilon_p}{2} = 0.29\ (2N_f)^{-0.405}$$

for nickel plated specimens with a coating thickness of approximately 2.5 μm.

Apparently, the cyclic strain coefficient, $\varepsilon_f'$, changes with different coating conditions. It has been shown that this value is equal to the monotonic fracture ductility, $\varepsilon_f$, in many cases. Since the monotonic fracture ductility virtually does not change with different surface coatings in the present study, this relationship is not applicable.

The cyclic stress-strain curves for the different systems are plotted in Figures 10-13. A series of cyclic stress-strain curves were also determined by multiple-step tests. In an attempt to make a close comparison of the cyclic behavior by ion plating, specimens used here were machined from the same single crystal rod. Each test started at $\frac{\Delta\varepsilon_T}{2} = \pm 1$ percent. When the initially saturated state was reached, the total strain amplitude was raised to ±2 percent and cycled to saturation. This procedure was repeated to ±3 percent and to ±4 percent. The cyclic

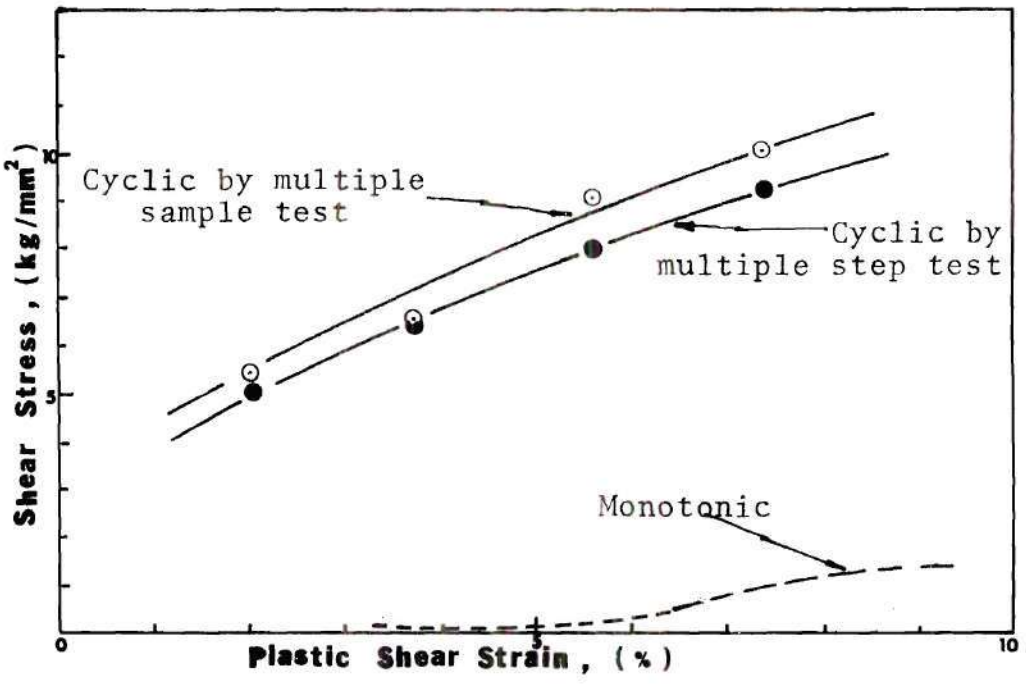


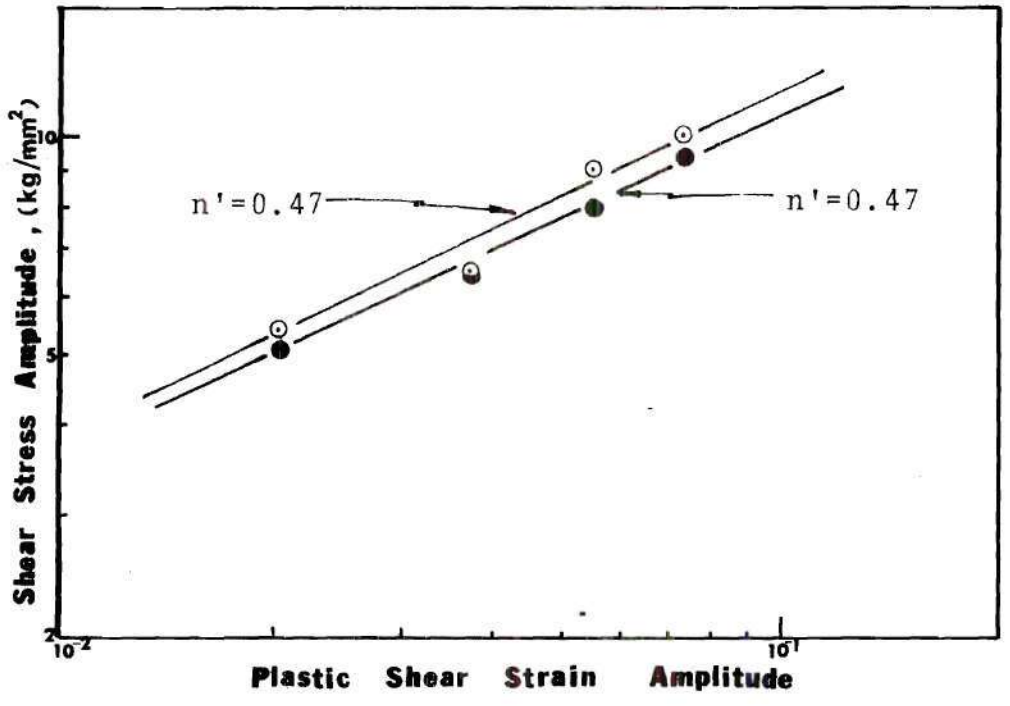


Figure 10. Cyclic Stress-Strain Curve of the Pure Copper Crystal

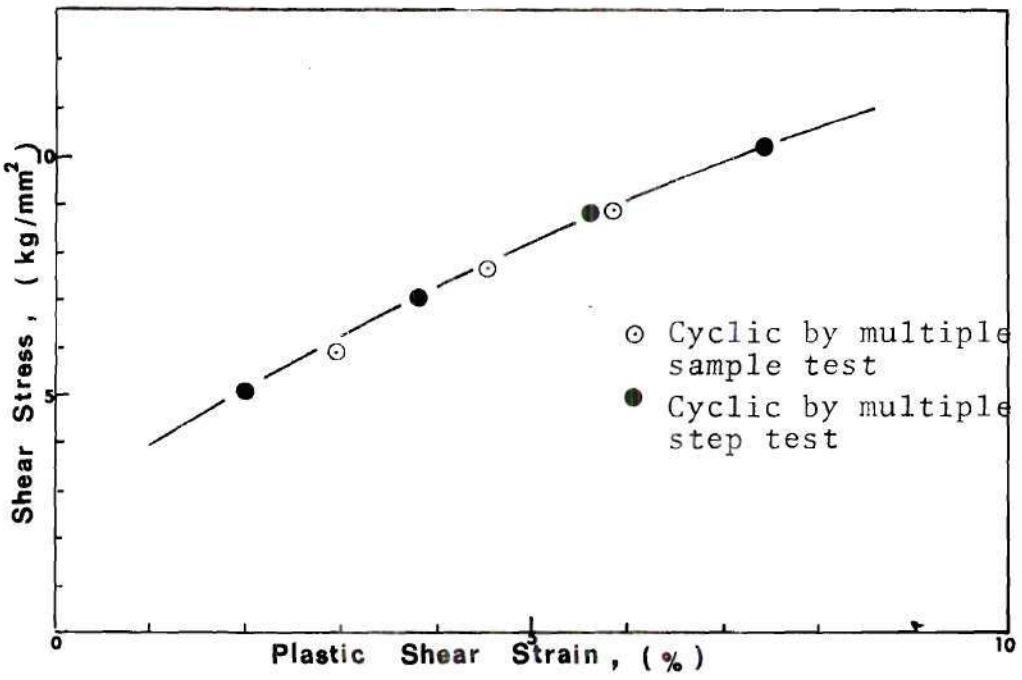


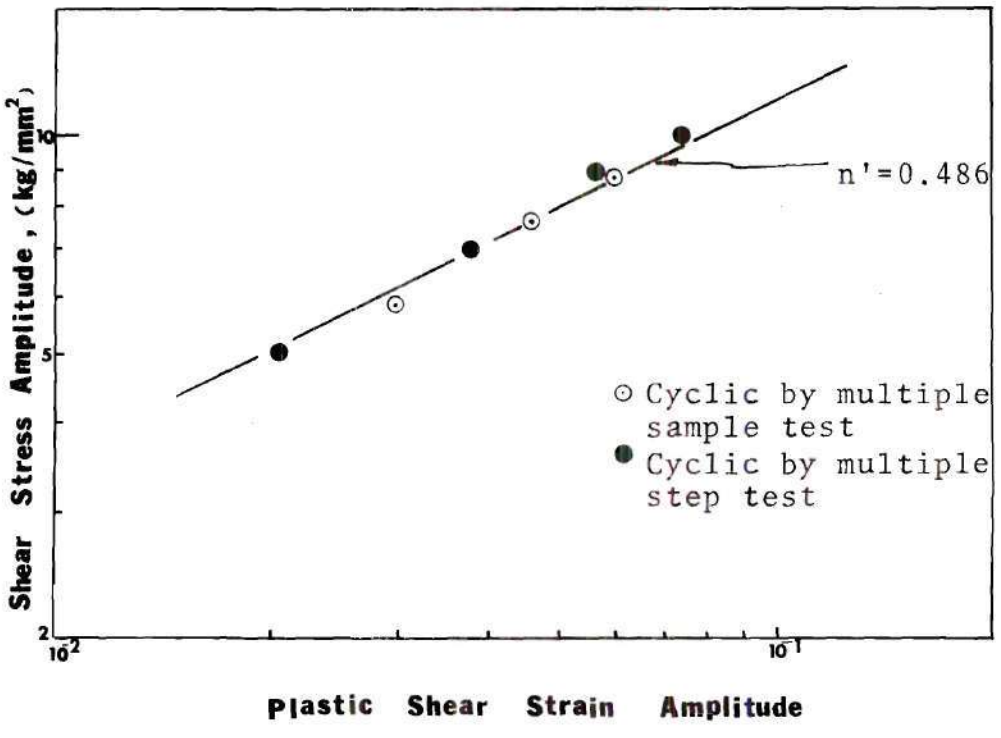


Figure 11. Cyclic Stress-Strain Curve of the Copper Plated Crystal

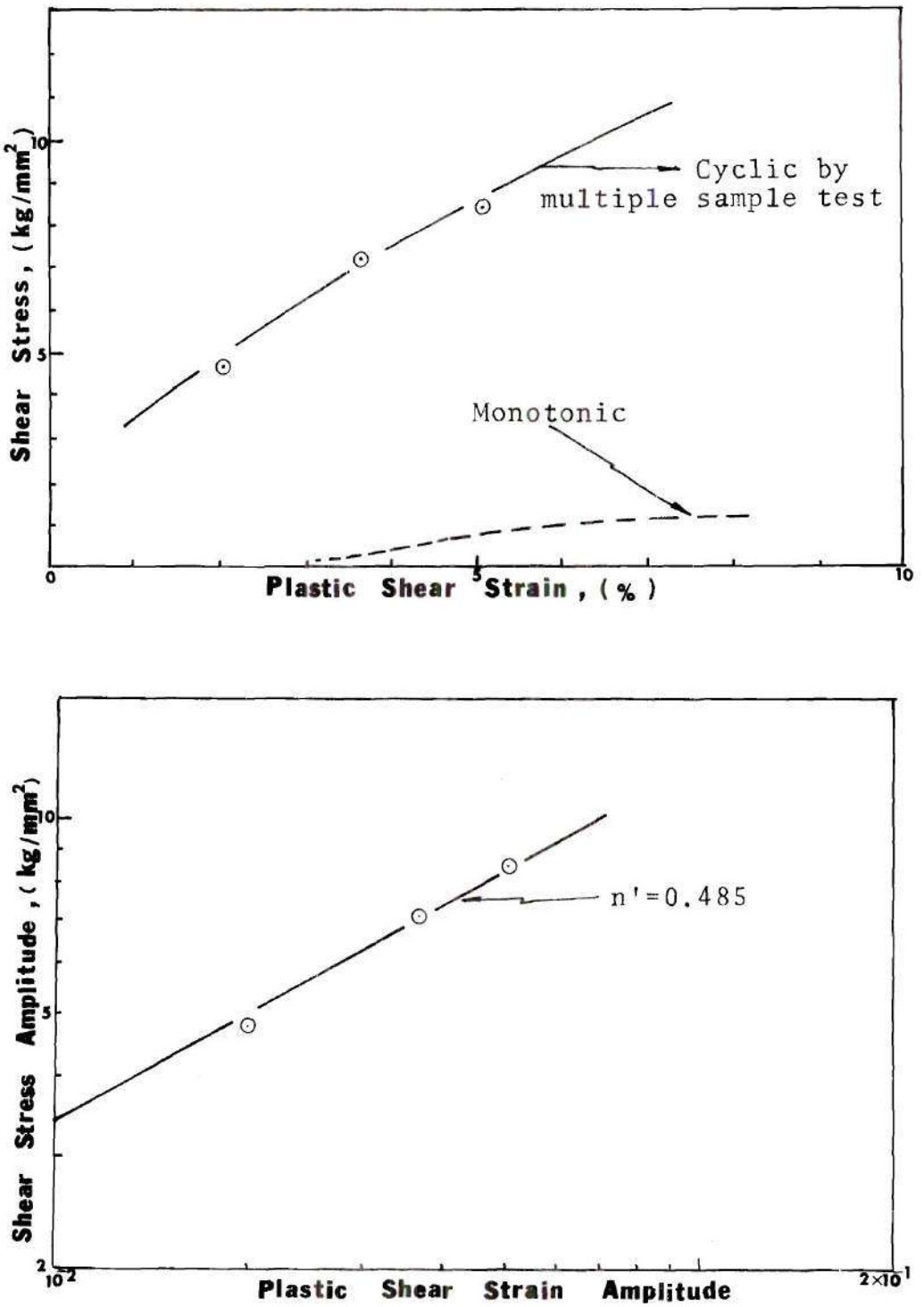


Figure 12. Cyclic Stress-Strain Curve of the Silver Plated Crystal

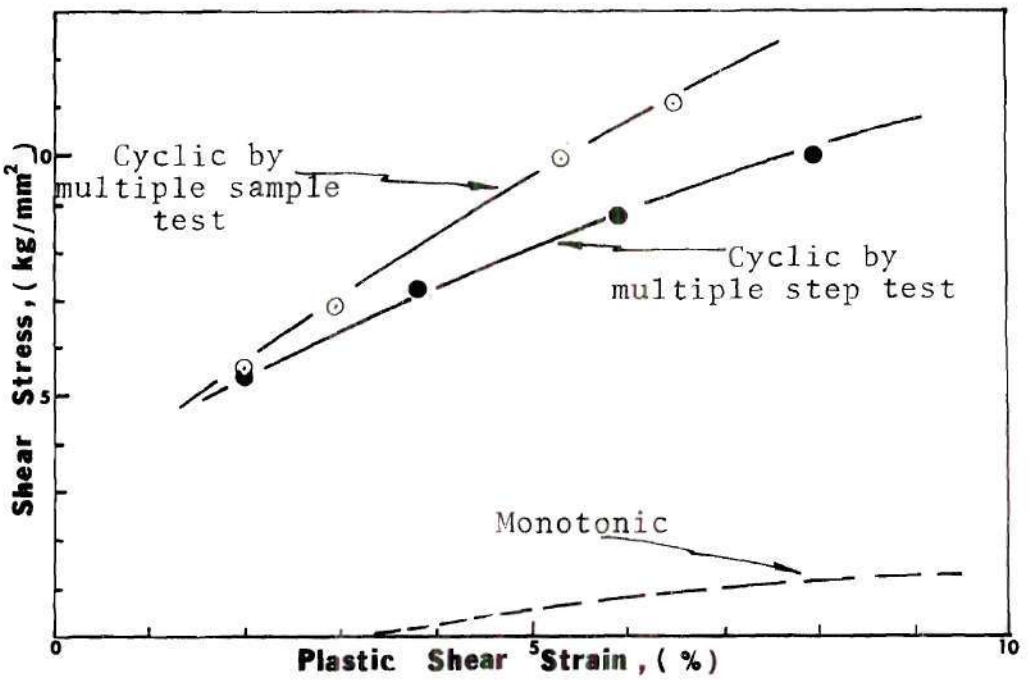


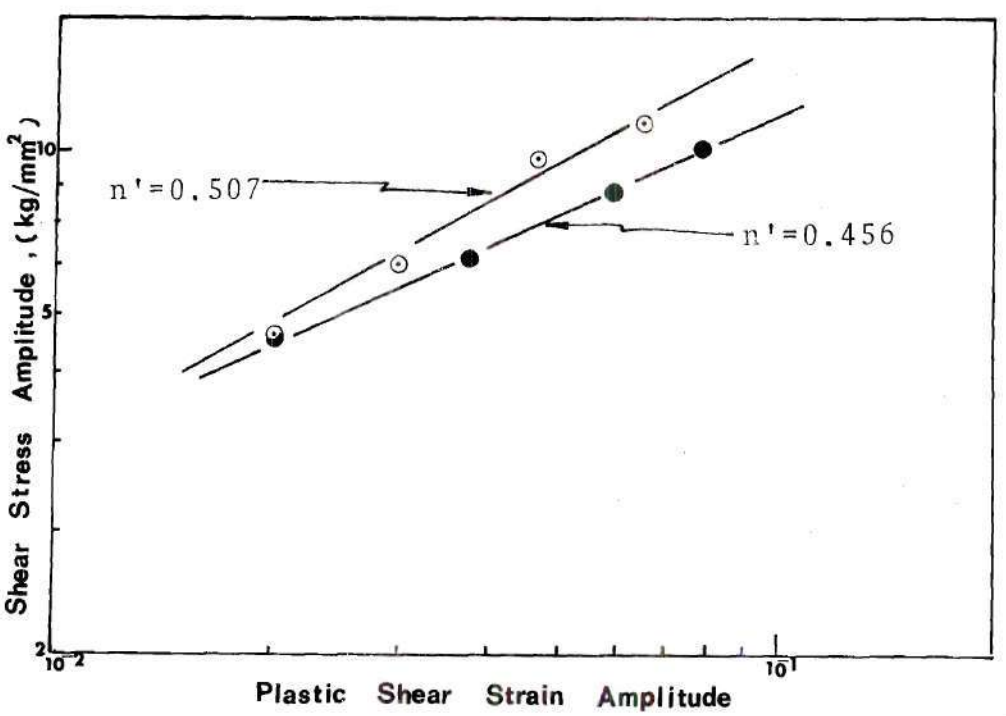


Figure 13. Cyclic Stress-Strain Curve of the Thick Nickel Plated Crystal

stress-strain curve was plotted by connecting the tips of the saturated loops. Figure 14 is an example demonstrating the multiple-step test on a pure copper crystal. There was a general tendency for the nickel plated specimen to always saturate at a higher stress than the pure copper specimen for the same strain amplitude.

## Surface Observation

Slip bands spread across the whole gauge section until the initial saturated state was reached. These bands belonged to the primary slip system and were uniformly distributed. Figure 15a is a scanning electron micrograph of pure copper surface after 30 cycles. As fatigue continued, slip traces of the secondary slip system were observed. However, the steps of these secondary surface markings were much shallower than the primary slip bands and were widely separated, Figure 15b. The superficial appearance of the original slip bands did not change appreciably, but it is evident that some slip bands become more active than the others. The step-heights of these bands increased gradually. As a consequence of the concentrated surface rumpling, microcracks were formed. Figure 15c is an example of the surface topography after 1200 cycles at $\frac{\Delta\varepsilon_T}{2} = \pm 1$ percent.

The surface observation described above are generally valid for all systems. Figure 16 and Figure 17 are respectively the silver plated and nickel plated crystals fatigued

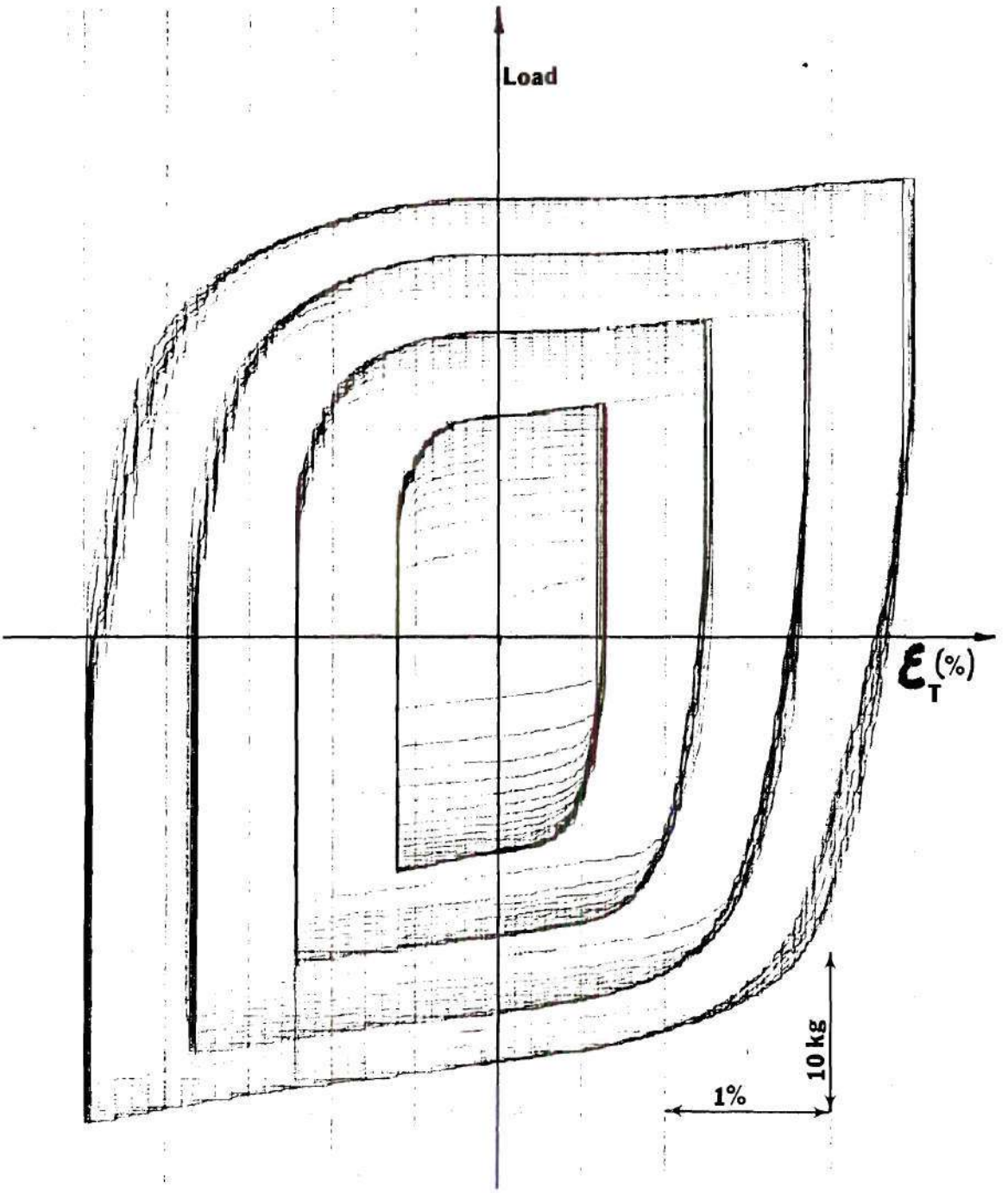


Figure 14. Hysteresis Loops Configurations for Plotting Cyclic Stress-Strain Curve by Multiple-Step Test

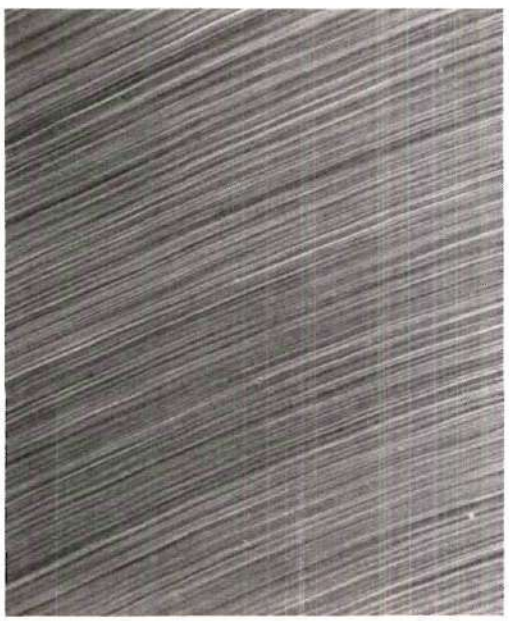

(a) 460x

(c) 935x

(b) 460x

Figure 15. Scanning Electron Micrograph of the Pure Copper Crystal Surface Fatigued at $\frac{\Delta\varepsilon_T}{2} = \pm 1$ Percent
(a) After 30 Cycles
(b) After 300 Cycles
(c) After 1200 Cycles

(a) 93x

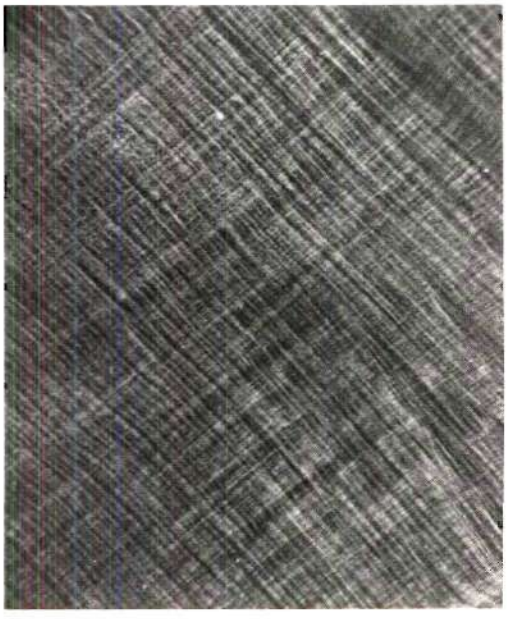

(c) 93x

(b) 93x

Figure 16. Scanning Electron Micrograph of the Silver Plated Crystal Surface Fatigued at $\frac{\Delta\varepsilon_T}{2} = \pm 1$ Percent
(a) After 30 Cycles
(b) After 300 Cycles
(c) After 1200 Cycles

(a) 460x

(c) 940x

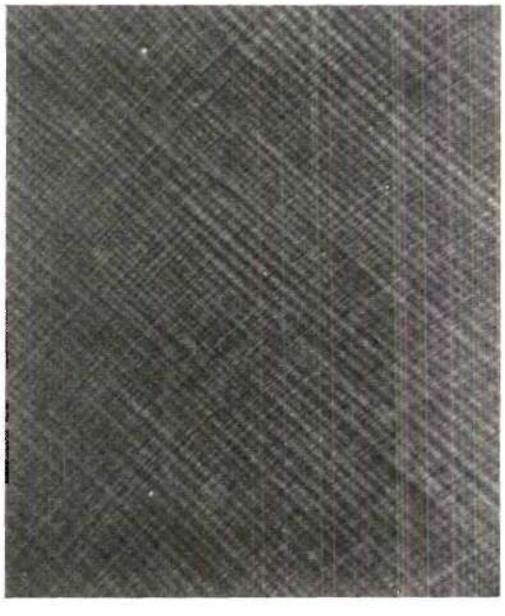

(b) 93x

Figure 17. Scanning Electron Micrograph of the Thin Nickel Plated Crystal Surface Fatigued at $\frac{\Delta\varepsilon_T}{2} = \pm 1$ Percent
(a) After 30 Cycles
(b) After 300 Cycles
(c) After 1200 Cycles

at the same conditions as the pure copper crystal shown in Figure 15. The similarity of slip traces of the coated surface with that of the uncoated crystal indicates that the coating film was epitaxial with the copper substrate. Otherwise, more random slip traces should have been observed on the coating film due to the Taylor criteria of polycrystalline deformation. The epitaxial nature of the coating was confirmed by both x-ray diffractometor traces and back reflection Laue patterns.

Figures 18a and 18b are the interferograms of the silver plated specimens after 300 and 1200 cycles fatigued at $\frac{\Delta\varepsilon_T}{2} = \pm 1$ percent. No quantitative measurement was made because of the limited focused area on such a small cylindrical surface. But qualitatively it indicated that the shifting of the interference fringes across some of the slip bands increased with the cycling. The step-height equals to $\lambda \cdot \frac{x}{2h}$, where $\lambda$ is the wavelength of the monochromatic mercury light (5460 Å), h is the measured spacing of the parallel fringes on the interferogram, and x is the displacement of the fringe across the slip band.[41]

The step-heights on the nickel plated surface are relatively higher than those of pure copper and silver plated specimens for the same strain amplitude and number of cycles. Figures 19a and 19b are the interferograms of nickel plated surface fatigued at the same condition as 18a and 18b. It shows that the characteristics of the slip bands on the

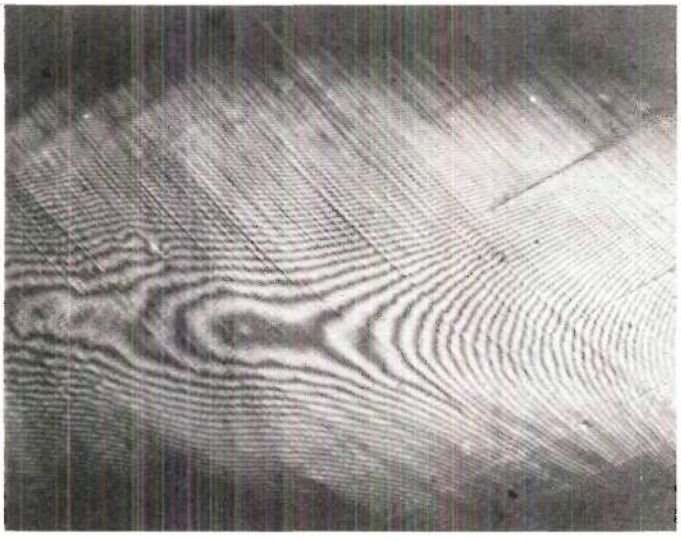

(a) 100x

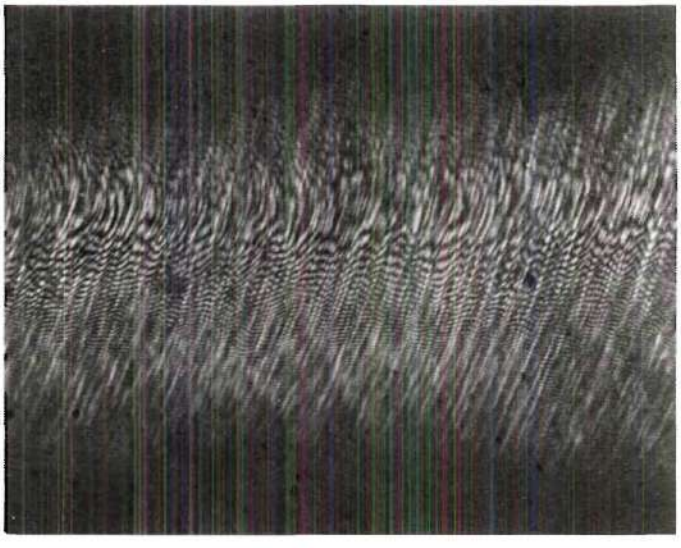

(b) 100x

Figure 18. Interferogram of the Silver Plated Crystal Fatigued at $\frac{\Delta\varepsilon_T}{2} = \pm 1$ Percent (a) After 300 Cycles, (b) After 1200 Cycles

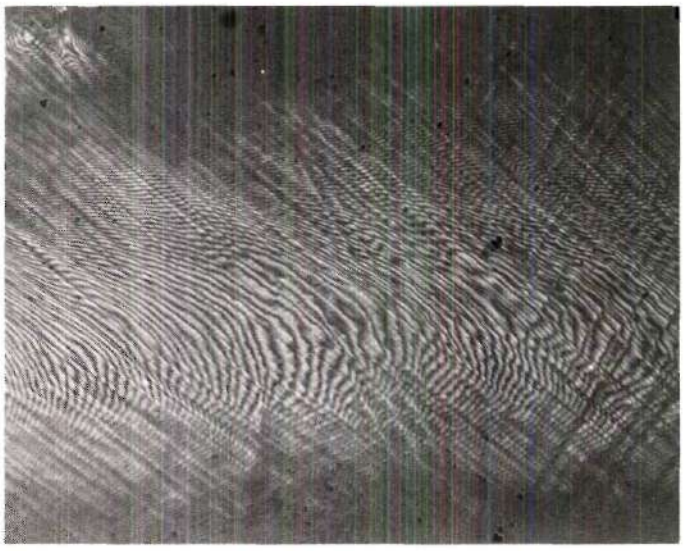

(a) 100x

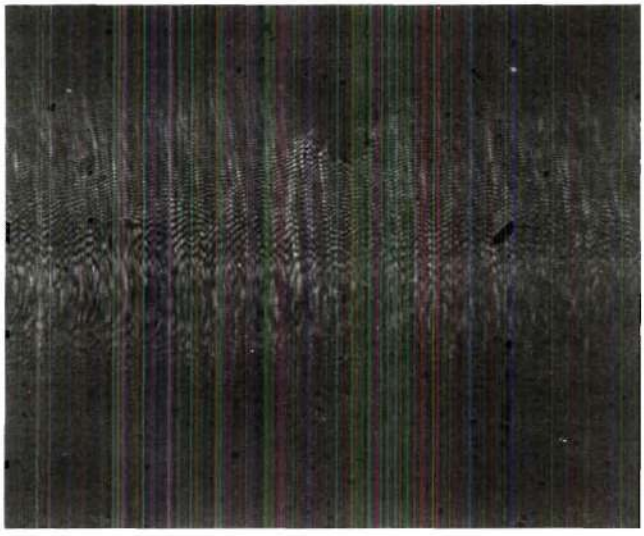

(b) 100x

Figure 19. Interferogram of the Thin Nickel Plated Crystal Fatigued at $\frac{\Delta\varepsilon_T}{2} = \pm 1$ Percent (a) After 300 Cycles, (b) After 1200 Cycles

surface can be changed by the different coatings.

## Transmission Electron Microscopy Observations

The transmission electron microscopy was performed near the center region of the sample, and no differences were detected in the structure of coated or uncoated samples. The following is a general description of what was observed for all samples as a function of cycles for a strain amplitude of $\frac{\Delta\varepsilon_T}{2} = \pm 1$ percent.

1. Observations after 30 cycles: The cyclic hardening rate was virtually equal to zero when the crystals were in the first saturation stage. The equiaxed dislocation cell structure becomes distinguishable on the primary slip plane, while on the conjugate slip plane, dislocations are densely concentrated in slabs roughly 4000 Å wide, and separated by regions of low dislocation density of approximately equal size. The cell walls and the dislocation slabs are mainly composed of tangled dislocations, but a large number of dislocation dipoles and prismatic dislocations are also visible, though in lower density. Figure 20a is an electron micrograph showing the dislocation arrangements on the (323) plane, which is 10.02 degrees from the primary slip plane, (111). Figure 20b shows the dislocation structure on the conjugate slip plane, $(\bar{1}\bar{1}1)$.

2. Observations after 300 cycles: At this stage, the fatigue softening rate was approaching zero. An elongated

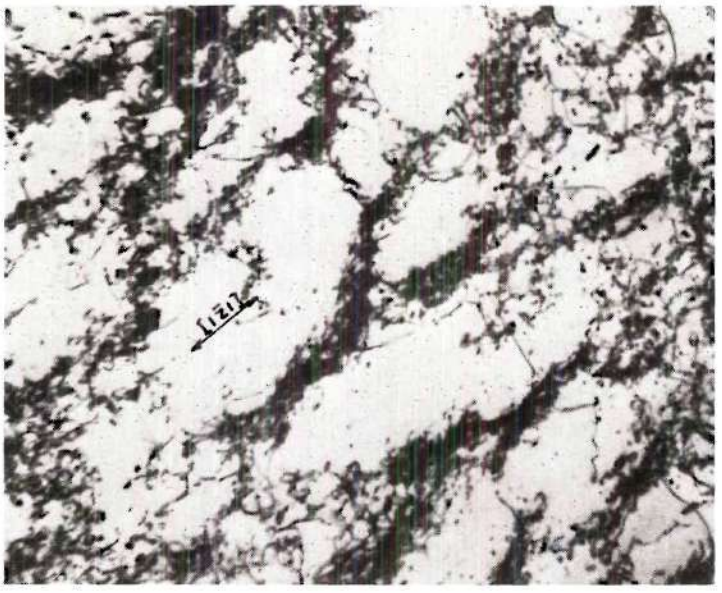


(a) 1 μm

(b) 1 μm

Figure 20. Transmission Electron Micrograph Showing Dislocation Structure in Fatigued Copper Crystal After 30 Cycles on (a) (323) Plane Which is 10.02° from the (111) Primary Slip Plane (b) ($\bar{1}\bar{1}$1) Conjugate Plane

cell structure is readily apparent on both the primary slip and the conjugate slip planes, Figure 21a and 21b. The cell wall width ranges from 2000 to 4000 Å. The average spacing between the walls is about 1 μm. The density of dislocation dipoles and loops in the cell walls have decreased substantially from that observed after 30 cycles. Tangled and jogged dislocations which fragmented into dense tangles of shorter segments now are the dominant features. Some dislocations lying across the interior of cells are seen on primary slip plane (Figure 21a). A very large number of round small black features are observed on the conjugate slip plane, Figure 21b. These have been previously suggested to be the agglomeration of point defects produced during fatigue.[42]

3. Observations after 1200 cycles: The cumulative strain ($\varepsilon_{cum}$) is 48 and the crystal is in the secondary hardening stage. Micrographs of (111) foils showed elongated cell structures with well defined cell walls lying along parallel to the $(1\bar{2}1)$ direction, Figure 22a. The interiors of cells are almost dislocation free. The dislocation density within the walls is so high that no individual dislocations can be distinguished. The misorientation between the cells apparently increases as the fatigue process continues. This can be deduced from the contrast difference across the cell walls. On the conjugate slip planes, the cell walls were not so well defined. There are scattered

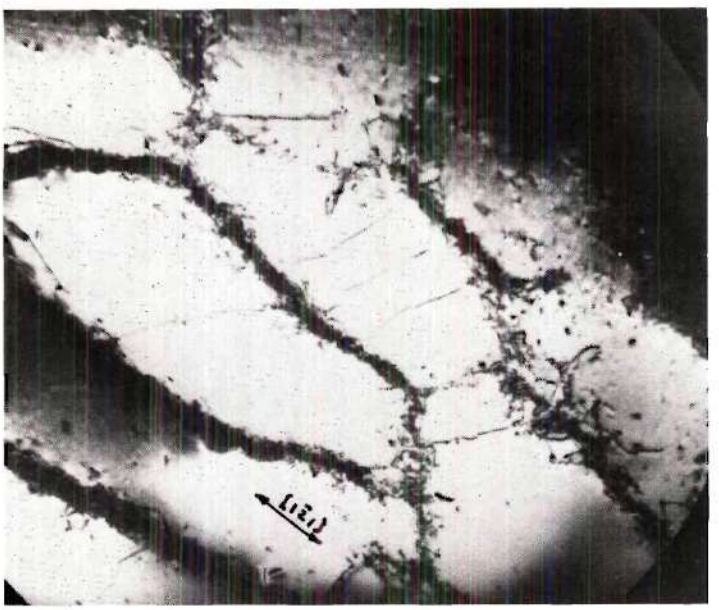


(a) 1 μm

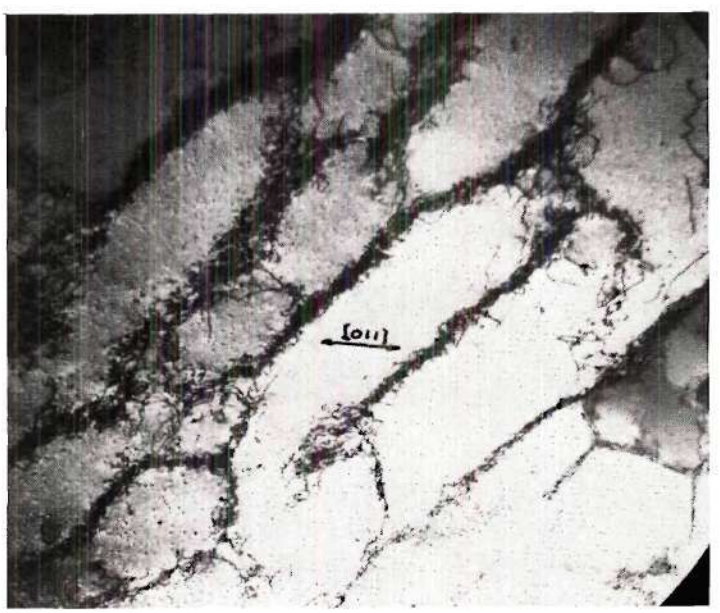


(b) 1 μm

Figure 21. Transmission Electron Micrograph Showing Dislocation Structure in Fatigued Copper Crystal After 300 Cycles on (a) (111) Primary Slip Plane (b) ($\bar{1}\bar{1}$1) Conjugate Plane

individual dislocations between the cell walls, and the cells are not so well aligned in an unidirection as was observed on the primary slip plane. Figure 22b is a micrograph of the $(\bar{3}\bar{2}3)$ plane, which is only slightly off the conjugate slip plane, $(\bar{1}\bar{1}1)$. On both the primary slip plane and the conjugate slip plane, microtwins were observed, Figure 22a, 22c. Since the formation of these twins can be produced only after large amounts of plastic deformation in copper crystals, these features were only observed after 1200 cycles of fatigue.

## Fracture

On the bases of metallographic observations, fatigue cracks normally propagate in two distinct stages after the crack initiation. The crack first propagates along the plane of maximum shear stress, stage I. This stage is followed by crack growth perpendicular to the applied tensile load, which is called stage II. In the present study, stage II crack propagation was the predominate mode, stage I crack propagation was insignificant by comparison.

Figure 23 is a typical fatigue-fracture surface of the copper crystal. It exhibits regularly spaced fatigue striations. These striations belong to type A, or the "ductile" type, each one consisting of a light and dark band, lying on the irregular non-crystallographic plateaux.[17] The arrow on the figure indicates the site of crack

(a) 1 μm

(b) 1 μm

Figure 22. Transmission Electron Micrograph Showing Dislocation Structure in Fatigued Copper Crystal After 1200 Cycles on (a) (323) Plane Which is 10.02° from the (1$\bar{1}$1) Primary Slip Plane (b) and (c) ($\bar{3}\bar{2}$3) Plane which is 10.02° from the Conjugate Plane ($\bar{1}\bar{1}$1)

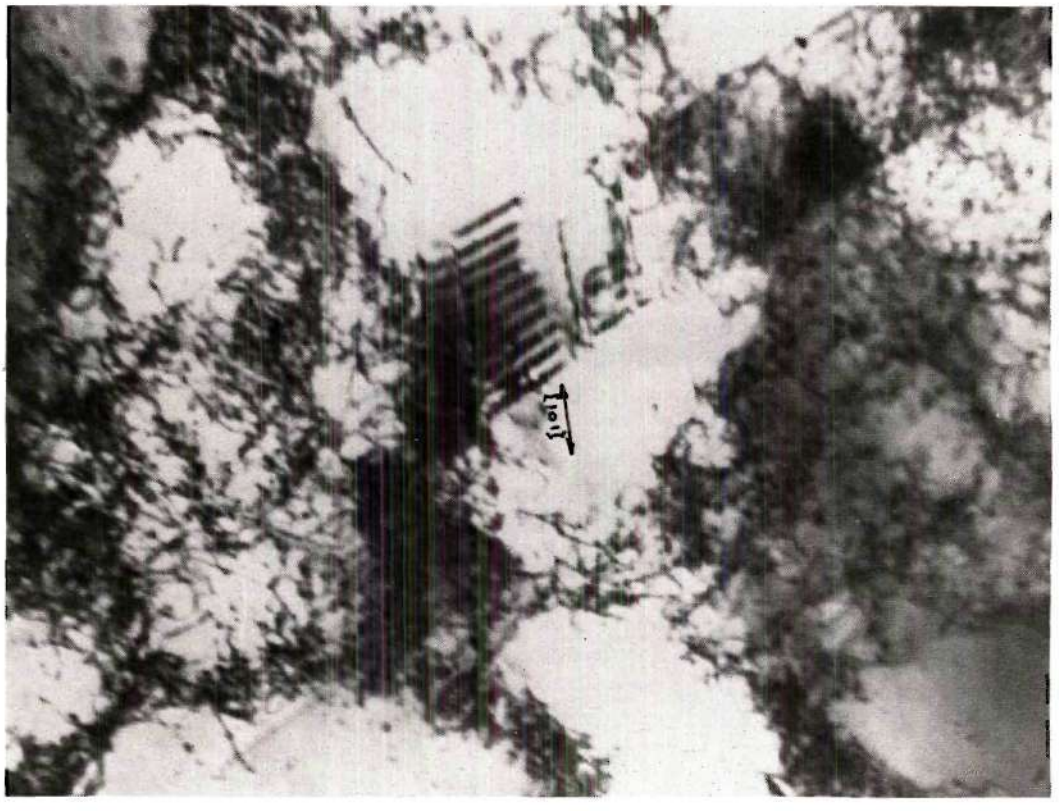


Figure 22. (continued)

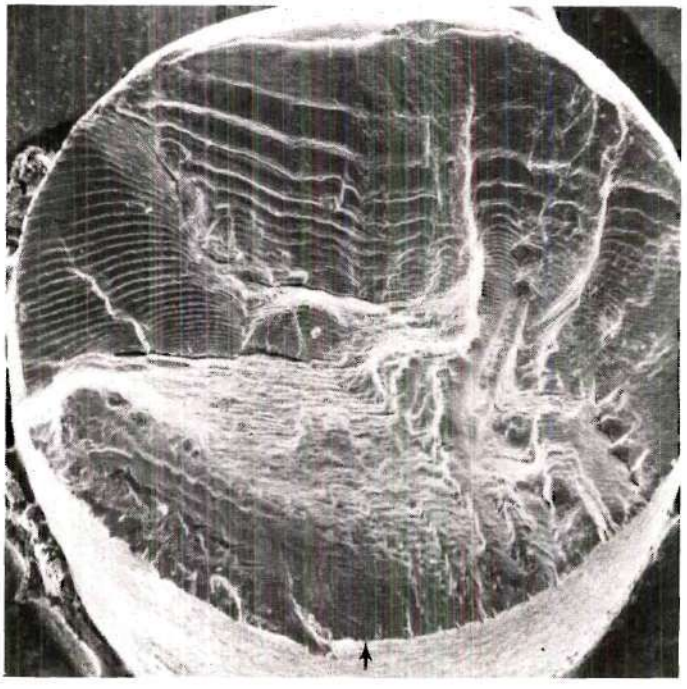

31x

Figure 23. Scanning Electron Fractograph of the Copper Crystal Fatigued at $\frac{\Delta\varepsilon_T}{2}$ = ±1 Percent

initiation. The direction of crack propagation is perpendicular to the striations. The spacing of the fatigue striations is closely related to the applied strain amplitude. This is clearly indicated by Figure 24, which is a nickel plated specimen, fatigued at $\frac{\Delta\varepsilon_T}{2} = \pm 3.5$ percent instead of the $\pm 1$ percent shown in Figure 23. The spacings are larger in Figure 23 than in Figure 22. Also, as the crack advances towards the bulk material, the striation spacing increases sharply. Back reflection Laue patterns taken from the fracture surfaces failed to reveal any sharp spots of the single crystal and the fracture plane at this stage could not be identified because of the extensive deformation.

The fracture surface of the ion-plated specimen did not show any separation between the coating film and the substrate crystal. It indicated the existence of a strongly adherent coating film and eliminated the possibility of fatigue crack initiated at the interface as has been observed in another investigation.[15]

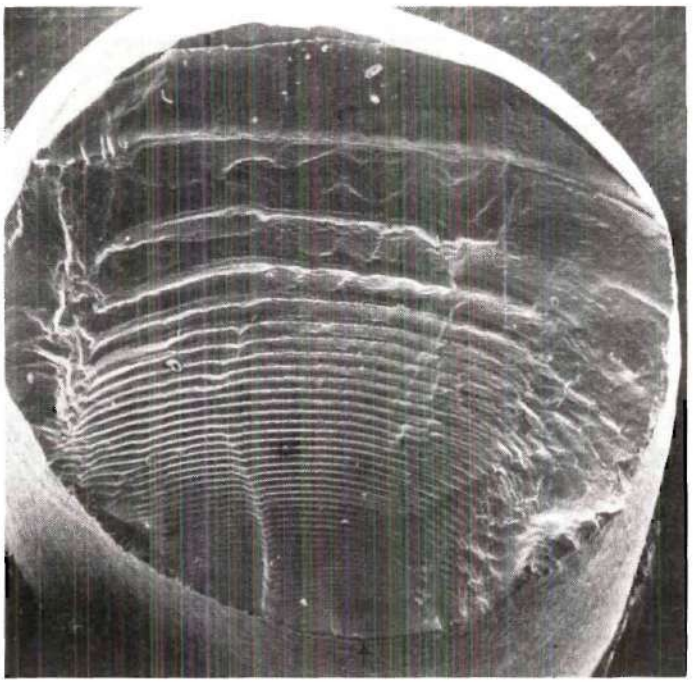

(a) 31x

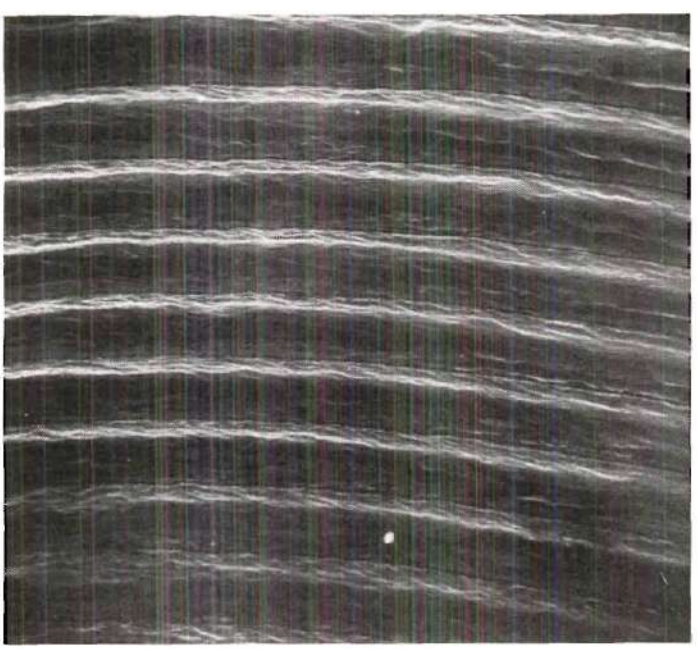

(b) 270x

Figure 24. Scanning Electron Fractographs of the Thick Nickel Plated Crystal Fatigued at $\frac{\Delta\varepsilon_T}{2}$ = ±3.5 Percent (a) and (b) show the same area but different magnification

# CHAPTER V

# DISCUSSION OF RESULTS

## Monotonic Property Changes Due to Ion-Plating

The deformation behavior of copper plated specimens was virtually identical with that of the uncoated specimens. This fact eliminated the possibility of effects due to impurities trapped in the interface from the ion-plating processes itself. Nickel plated and silver plated specimens showed appreciable changes in the critical resolved shear stress. The direct load sharing capacity of the coating film was negligible and should have contributed only 0.3 percent of the measured strength. Nickel and silver are both face center cubic, as is copper, and the lattice parameters of these three metals are close.[43] Therefore, strengthening due to crystal structure differences and coherency strains at the interface are quite unlikely. The remaining possible strengthening mechanisms are from solid-solution hardening and from elastic modulus changes between the film and the substrate.

In ion plating, a solid solutioned layer can be created from two sources: firstly, by the direct penetration of the solute material, and secondly, by the limited solid diffusion. The depth of penetration depends on the mass of

incident ionized particles, the mass of the substrate ions and the energy of the incident ions. The mean ranges in a large number of crystal systems have been measured as 10-100 Å/keV.[44] In the present study, the maximum potential applied was 3.5 kV, and the depth of penetration of the coating material was expected to be small. During sputtering the ionized particles with high velocity are stopped by the substrate and give up their kinetic energy, mostly in the form of heat. The surface temperature of the specimen during plating could reach about two hundred degrees centigrade. As soon as the ion plating was finished and the ionization current cut off, the temperature on the surface dropped rapidly. The length of time the specimens stayed at the upper temperature level where diffusion might occur was quite short. The thickness of the solid-solutioned layer here was thin (of the order of 100 Å) when compared with that obtained by Patterson and Greenfield[6] (0.4 to 2 μm) and it was felt that solid solution strengthening could be ignored. However, the thin solid-solutioned layer still plays an important role during plastic deformation. The coherency of the coating film with the substrate enables them to deform as a continuum and peeling and scaling of the surface coating was not observed during plastic deformation.

The shear modulus of nickel is $7.4 \times 10^{11}$ dyne/cm$^2$, copper is $4.8 \times 10^{11}$ dyne/cm$^2$, and silver is $3.0 \times 10^{11}$ dyne/cm$^2$. In other words, the shear modulus of nickel is

54 percent higher than copper, and that of silver 38 percent lower. As discussed previously in reference 5, an increase of the critical resolved shear stress of the nickel plated specimen is expected. By the same token, the critical resolved shear stress should be decreased by the silver coating. The experimental results of this study support these previous conclusions.

It seems that the surface coating can change the deformation behavior not only in its early stages, but also in stage III. Similar results have been reported,[5,6] but no mechanism for this behavior has been proposed. The effect of surface coating on stage III plastic deformation is too complicated to be analyzed. The role of individual strengthening mechanisms caused by surface coating on different slip systems which are operating at the same time at this stage is difficult to assess.

## Residual Stresses by Ion-Plating

In the present study, the coating atoms are only substitutionally dissolved in the copper substrate. The atomic size factors of the present coupling systems are all within Hume-Rothery's 15 percent limit. The atomic radius of copper is 1.28 Å, which is 11 percent smaller than silver's 1.44 Å and 2.4 percent larger than nickel's 1.25 Å.[43] Therefore, the Ag-Cu interface should be in a state of tensile strain, and the Ni-Cu interface should be

in compressive strain. It is well known that tensile strains are detrimental to the fatigue behavior, while compressive strains are beneficial. The experimental results are in the opposite direction and support our earlier contention that these strains are insignificant when compared with the other factors. The calculated root mean square residual strain was very small, of the order of $10^{-4}$. This may be the real value, however, it may also be due to the small affected zone as compared with the penetration depth of the x-rays. The penetration depth for Cu radiation in copper is roughly 18 μm, while for pure nickel it is roughly 19 μm.

Residual stresses are normally intended to resist stress cycling. In strain-controlled tests, especially in the low cycle fatigue range, residual stresses will be relaxed rather quickly, and this fact also minimizes their importance in the present study.

## Fatigue Hardening and Softening

Low cycle fatigue tests conducted in this study were quite different from most of the previous work. The minimum total strain amplitude used here is ±1 percent, which was equivalent to a total shear strain amplitude of ±2.03 percent. Feltner and Laird[45] defined large strain amplitudes as those values which caused fatigue failure in less than $5 \times 10^4$ cycles. However, in the present study, the maximum fatigue life obtained from a silver plated specimen fatigued at

$\frac{\Delta\varepsilon_T}{2}$ = ±1 percent was 4 x $10^3$ cycles. It was still an order of magnitude less than the limit of Feltner and Laird's definition. So, the present study should possibly be called "very high strain amplitude fatigue."

There are scattered reports on low cycle fatigue behavior with strain amplitudes in the same range of the present study.[29,46] However, all systematic studies have been conducted in the range far below ±1 percent of total strain amplitude. It has been agreed that a high stacking fault energy material, such as copper, initially in the annealed state, will go through rapid strain hardening and saturation stages during a low cycle fatigue test. When the saturation stage is reached, the corresponding stress amplitude remains constant with further cycling, and the magnitude is determined only by the strain amplitude and the temperature.[46,47] The hysteresis loops were observed to be symmetrical in tension and compression after only a few cycles.[46] In the present study, after an initial saturated state, fatigue softening occurred and lasted for some time followed by secondary hardening and finally fracture. Since this behavior had not been reported before, it was first thought to be due to experimental error. However, with further study, it was proved to be a reproducible phenomenon. For those cases with $\frac{\Delta\varepsilon_T}{2}$ > ±2 percent, no secondary hardening occurred because of early crack formation. Roberts[29]

mentioned a similar fatigue softening phenomenon in his stress-controlled fatigue work, but did not elucidate the phenomenon.

There have been many attempts made to correlate the fatigue saturation with the dislocation arrangements. Some models have been designed to provide a mechanism whereby non-hardening reversible plastic strain could occur. The earliest model was proposed by Feltner[48] who suggested that the saturation strain could be accommodated by the flip-flop motion of dislocation dipoles. This idea was derived from observations of numerous dislocation dipoles in the fatigued crystal. There are two major mechanisms for the formation of dislocation dipoles in fatigue. The first one involves the cross slip of screw dislocations; the loops being dragged out from a sessile jog on the screw dislocation and terminated by cross slip.[49] The second one is by mutual trapping of edge dislocations of opposite sign.[50] There is no doubt about the existence of dislocation dipoles in the present study, but the high dipole density and uniformity required by Feltner's model is not supported by our observations. Furthermore, the concept of his model requires that the plastic strain is contributed by the flip-flop motion of the dislocation dipoles between equilibrium positions, and is essentially completely reversible, which would negate any further softening. Feltner's model may be more valid for low strain amplitude fatigue.

Another model is the cell shuttling model[51] in which the plastic strain is provided by the to-and-fro motion of dislocations between the cell walls. The estimated number of dislocations which must shuttle to accommodate the plastic strain is reasonable. Only 5 percent of the total dislocations is needed for copper fatigued at $\frac{\Delta\gamma_T}{2} = \pm 0.75$ percent.[51] This model satisfactorily explains the accommodation of plastic strain during fatigue saturation, but the calculated flow stress is much lower than the observed value.[2] Figure 17b clearly shows straddling dislocations between the cell walls, and suggests that a cell shuttling mechanism may play a role in the cyclic behavior of the present study.

A point-defect cluster hardening model has been suggested[2] in which the saturation stress of the fatigued crystals is controlled by the internal stresses and defect clusters within the interior of the cells which impede dislocation motion through these regions. The point defects are generated during the early stage of fatigue and later convert into clusters. Piqueras et al.[52] used the weak beam transmission electron microscopy technique to determine the size and density of defect clusters in copper single crystals fatigued to saturation. A quantitative analysis of the yield stress temperature relationship made them believe that this model was the governing one for saturation stress in metal fatigue. However, Finney and Laird[28] suggested that their measurement of the density of point-defect clusters in the

areas between the walls was not very precise. In the present study, numerous point-defect clusters were also observed, however, no quantitative analysis was made. Therefore, no contribution in this respect can be given.

The fatigue softening and the secondary hardening were found after the initially saturated state was reached. In the strain-controlled fatigue test, this phenomenon was shown on the curve of the stress amplitude versus the number of cycles. The peak stress amplitude decreased slightly with further cycling after the initially saturated state. It decreased to a minimum and then increased again. This observation was assumed to be the result of the very high strain amplitudes used in this study, and associated with duplex slip.

When the initial saturated state is approached, the strain hardening rate is almost zero, and the dislocation arrangement still does not show a well defined 3-D cell structure. In the conventional high strain amplitude fatigue studies, cell structures are quite evident.[51,53] The microstructure we observed in the initial saturated state, Figure 20a and 20b, is believed to be metastable. As cycling continues, slip on secondary slip systems becomes more active. Cross-slip processes can easily occur and dynamic recovery, as in stage III of unidirectional deformation, occurs. The flow stress is decreased by the annihilation of dislocations and by their rearrangement into lower-energy configurations.

However, at the same time, a competing hardening mechanism is also functioning. Dislocations activated on the secondary slip systems must cut through the existent dislocation bundles which serve as obstacles. Bundles of secondary dislocations are also formed and act as the obstacles to the existent dislocations. The effect of this mutual trapping mechanism is an increase of resistance to plastic flow. The overall fatigue behavior after the initially saturated stage is therefore the net result of the softening and the hardening mechanisms contributed by duplex slip. During fatigue softening, apparently the former mechanism overcomes the latter. The dislocation density continues to increase as does the number of associated dislocation barriers. When the density of dislocation barriers reaches a threshold value, secondary fatigue hardening predominates.

The difference in the fatigue behavior observed in the present study and previous investigations is believed to be a result of the higher strain amplitudes used in this work. Duplex slip systems become more active as the fatigue strain amplitude is increased. No drastic change of fatigue hardening or softening mechanisms are proposed.

## Fatigue Lives Changed by Ion-Plating

Surface coatings used for changing the fatigue lives represent a practical means for controlling crack initiation. It is well established that increasing or decreasing crack

initiation times usually have significant effects on the total fatigue life only in high cycle fatigue range.[54] Many observations have been made which suggests that in the low cycle fatigue range, cracks are initiated in the very early stage of the fatigue life. The present observations seem contrary to this fact. We have observed a ratio of the number of cycles for crack initiation (No) to the total number of cycles to failure (Nf) ranging from 35 percent to 80 percent. The ratio depends on the strain amplitude used. With the higher strain amplitude, the No/Nf ratio becomes lower. Similar results were found in Chien's recent work on the effect of ordering on the low cycle fatigue of $Cu_3Au$.[3] The discrepancy between our work and previous results can be explained as follows:

Firstly, it may be associated with the definition of the crack. Presently, there is no mutual agreement among investigators about this term. The initial crack may be defined as long as 3 mm by someone, or 1000 Å by someone else. In the present study, crack initiation is defined when a "crack" appears which can be observed by the naked eye, which is roughly a few tenths of a millimeter. For example, in Figure 17c, it is apparent that microcracks, as indicated by the arrows, have formed after 1200 cycles on a nickel plated specimen, but these were only barely detected by the naked eye.

Secondly, the specimen in the present study was

carefully chosen and prepared to reduce the number of possible crack initiation sites. Fatigue cracks were only found to be initiated at the slip bands. However, in previous work, crack initiation could have taken place at many structural weaknesses such as grain boundaries, twin boundaries, inclusions or second-phase particles, etc.

Fatigue lives of some ion plated specimens were changed in the present study as described in the last chapter. The copper plated specimens did not show any significant change from the uncoated specimens. One must conclude, therefore, that the increase of fatigue life by silver plating and the decrease by nickel plating are due to the different properties of the coating material. In all cases of the present study, cracks initiated in the slip bands and were observed first on the thick nickel plated specimens, next on the thin nickel plated specimens, then on the pure copper specimens, and finally on the silver plated specimens under similar conditions. Therefore, it is believed that the different coatings can change the characteristics of the slip bands on the surface. Nickel seems to promote the heterogeneity and irreversibility of plastic strain on the surface, and it becomes more phenomenal with the increase of coating thickness. Silver appears to retard it.

The difference mentioned above has been studied on pure materials with different slip modes;[55] but no one has indicated that this could also happen in a composite system.

A planar slip mode is displayed by those metals or alloys of low stacking fault energies which inhibit easy cross-slip. Cross slip is believed to play an important role in the formation of persistent slip bands. Avery et al.[56] showed that the rate of extrusion and intrusion on copper crystals was sharply changed with the resolved shear stress on the cross-slip plane. This was accomplished by orienting two crystals in such a way that the resolved shear stresses on the primary slip plane was essentially the same while the shear stresses on the cross-slip plane were varied by a factor of 10. The crystal with the higher cross-slip stress developed the persistent slip bands much faster than the other one. Recently, Saxena and Antolovich[34] found that lowering the stacking fault energy of Cu-Al alloys, resulted in significant improvements in fatigue properties. Their work was conducted in the low cycle fatigue range. Earlier, Avery and Backofen[33] worked on the same alloy system, but in the high cycle fatigue range. The increase of fatigue lives were even more drastic.

The stacking fault energy of silver is 21.6 ergs/cm$^2$, copper is 55 ergs/cm$^2$, and nickel is 225 ergs/cm$^2$. These values are taken from Gallagher's paper of 1970,[57] which might be somewhat different from other sources.[23,58,59] However, the sequence of the magnitude of these values is consistent. For the silver plated system, the slip mode in the coating film is more planar than in the coated substrate.

For the nickel plated system, the slip mode in coating film is more wavy than in the substrate. The change of slip mode across the interface alters the characteristics of slip steps on the surface, and therefore the cycles for crack initiation. Due to extreme experimental difficulties, the microstructure of the coating film was not examined. The exact mechanism of the slip-step changes is still unknown.

It should be emphasized that these results may not apply to all systems. Surface coating materials of different stacking fault energies will not necessarily change the low cycle fatigue lives. Low cycle fatigue tests were conducted on a series of polycrystalled aluminum specimens and also on aluminum specimens ion plated with copper. The results (Table 3) were scattered, and no general conclusion could be drawn. For both groups of specimens, crack initiation occurred at the grain boundaries and the surface rumpling was large, and the total fatigue lives were much shorter than those of single crystals. However, further work in this area is still underway by other workers,[60] and no definite conclusions as to the influence of varying the stacking fault energy of the surface of polycrystalline samples can be made at this time. Some improvements may be obtained in the high cycle region, however, presently this would only be speculative.

Table 3. Low Cycle Fatigue Lives for Cu Coated and Uncoated Al Specimens

| Specimen | $\frac{\Delta\varepsilon_T}{2}$ (±%) | $N_f$ (cycles) |
|---|---|---|
| Uncoated | 0.77 | 1,370 |
| | 1 | 807 |
| | 2 | 214 |
| | 3 | 63 |
| Coated | 0.77 | 1,473 |
| | 1 | 735 |
| | 2 | 223 |
| | 3 | 108 |

# CHAPTER VI

## CONCLUSIONS

Based on the experimental results of the present study, the following conclusions can be drawn with regard to the ion-plating effects on unidirectional tensile and low cycle fatigue behavior of copper single crystals. Nickel, silver and copper were used as the coating materials.

1. The unidirectional deformation behavior is changed and depends on the properties of the coating materials. For the systems studied, the elastic modulus difference between the coating film and the substrate is the dominent factor, and increases or decreases in critical resolved shear stress occur depending on whether the modulus is higher or lower than the substrate.

2. The ion-plating process itself does not significantly effect the deformation behavior in unidirectional tensile and low cycle fatigue tests.

3. Surface residual stresses produced by ion plating were insignificant in the present study.

4. Initial fatigue hardening was observed followed by a saturated period, fatigue softening and secondary hardening. This is associated with the very high strain amplitude applied in the present study and the considerable

duplex slip.

5. The low cycle fatigue life is increased by silver plating, while it is decreased by nickel plating. The difference is a result of fatigue crack initiation being retarded by a low stacking fault energy coating, or promoted by a high stacking fault energy coating.

# BIBLIOGRAPHY


1. T. Spalvins, NASA TM X-52859 (1970).

2. J. C. Grosskreutz, Phys. Stat. Sol. (b), Vol. 47 (1971), 11.

3. K. H. Chien, Ph.D. Thesis (1974), Georgia Institute of Technology.

4. H. D. Nine and H. M. Brandler, Acta Met., Vol. 12 (1964), 895.

5. B. R. Livesay and E. A. Starke, Jr., Acta Met., Vol 21 (1973), 244.

6. W. R. Patterson and I. G. Greenfield, Acta Met., Vol. 19 (1971), 123.

7. L. C. De Jonghe and I. G. Greenfield, Acta Met., Vol. 17 (1969), 1411.

8. I. R. Kramer, Trans. Met. Soc. AIME, Vol. 227 (1963), 1003.

9. I. R. Kramer, Trans. Met. Soc. AIME, Vol. 230 (1964), 991.

10. H. Shen, S. E. Podlaseck, and I. R. Kramer, Trans. Met. Soc. AIME, Vol. 233 (1965), 1933.

11. P. G. Fluck, Proc. ASTM, Vol. 51 (1951), 584.

12. R. J. Love, Symp. Properties of Metallic Surfaces, Inst. of Metals, Vol. 161 (1952).

13. J. C. Grosskreutz and D. K. Benson, Surfaces and Interfaces II, Syracuse University Press (1968), p. 61.

14. R. A. F. Hammond and C. F. Williams, Met. Rev., Vol. 5 (1960), 165.

15. I. G. Greenfield and D. N. Snyder, AD-755 385, 1973.

16. I. R. Kramer, Technical Report AFML-TR 69-182, 1969.

17. W. J. Plumbridge and D. A. Ryder, Met. Rev., Vol. 14 (1969), 119.

18. J. A. Ewing and J. W. Humphrey, Phil. Trans., Vol. 200 (1903), 241.

19. P. J. E. Forsyth, J. Inst. Metals, Vol. 83 (1954-1955), 395.

20. A. H. Cottrell and D. Hull, Proc. Roy. Soc., Vol. 242 (1957), 211.

21. N. Thompson, N. J. Wadsworth, and N. Louat, Phil. Mag., Vol. 1 (1956), 113.

22. T. H. Alden and W. A. Backofen, Acta Met., Vol. 9 (1961), 352.

23. W. A. Wood, "The Study of Metal Structures and Their Mechanical Properties," Pergamon Press, 1971.

24. P. J. E. Forsyth, Proc. Roy. Soc., Vol. A 242 (1957), 198.

25. E. E. Laufer and W. N. Roberts, Phil. Mag., Vol. 14 (1966), 65.

26. D. F. Watt and R. K. Ham, Nature (London), Vol. 211 (1966), 734.

27. P. J. Woods, Phil. Mag., Vol. 28 (1973), 155.

28. J. M. Finney and C. Laird, Phil. Mag., Vol. 31 (1975), 339.

29. W. N. Roberts, Phil. Mag., Vol. 20 (1969), 675.

30. P. Lukas, M. Klesnil, and J. Krejel, Phys. Stat. Sol., Vol. 27 (1968), 545.

31. R. L. Segall, Adv. Mater. Res., Vol. 3 (1968), 109.

32. J. T. McGrath and R. C. A. Thurston, Trans. Met. Soc. AIME, Vol. 227 (1963), 645.

33. D. H. Avery and W. A. Backofen, "Fracture of Solids," Vol. 20 (1963), 339.

34. A. Saxena and S. D. Antolovich, Trans. Met. Soc. AIME, (in press).

35. H. I. Kaplan and C. Laird, Trans. Met. Soc. AIME, Vol. 239 (1967), 510.

36. C. Laird, ASTM STP No. 415, Am. Soc. Testing Mat., 1967, 131.

37. B. E. Warren, "X-Ray Diffraction," Addison-Wesley, 1969.

38. W. A. Rachinger, J. Scient. Instrum., Vol. 25 (1948), 254.

39. A. R. Stokes, Proc. Phys. Soc., Vol. 61 (1948), 382.

40. B. Rossi, "Optics," Addison-Wesley, 1957.

41. V. A. Phillips, "Modern Metallographic Techniques and Their Applications," Wiley-Interscience, 1971.

42. S. J. Basinski, Z. S. Basinski, and A. Howie, Phil. Mag., Vol. 19 (1969), 899.

43. M. Hansen, "Constitution of Binary Alloys," McGraw-Hill, 1958.

44. G. Carter, J. Vac. Sci. and Tech., Vol. 7 (1970).

45. C. E. Feltner and C. Laird, Acta Met., Vol. 15 (1967), 1633.

46. C. E. Feltner and C. Laird, Acta Met., Vol. 15 (1967), 1621.

47. C. E. Feltner and C. Laird, Trans. Met. Soc. AIME, Vol. 242 (1968), 1253.

48. C. E. Feltner, Phil. Mag., Vol. 12 (1965), 1229.

49. W. G. Johnston and J. J. Gilman, J. Appl. Phys., Vol. 31 (1960), 632.

50. A. S. Tetelman, Acta Met., Vol. 10 (1962), 813.

51. J. R. Hancock and J. C. Grosskreutz, Acta Met., Vol. 17 (1969), 77.

52. J. PiQueras, J. C. Grosskreutz and W. Frank, Phys. Stat. Sol., Vol. 11 (1972), 567.

53. C. R. Gostelow, Metal Sci. J., Vol. 5 (1971), 177.

54. L. F. Coffin, Jr., Annual Rev. of Mat. Sci., Vol. 2 (1972), 313.

55. A. J. McEvily and T. L. Johnston, Int. Conf. on Fracture, Sendai (1965), 515.

56. D. H. Avery, G. A. Miller, and W. A. Backofen, Acta Met., Vol. 9 (1961), 892.

57. P. C. J. Gallagher, Met. Trans., Vol. 1 (1970), 2429.

58. R. E. Smallman and K. H. G. Ashbee, "Modern Metallography," Pergamon Press, 1966.

59. J. Friedel, "Dislocations," Pergamon Press, 1967.

60. J. T. Staley, T. H. Sanders, D. A. Mauney, and E. A. Starke, Jr., private communication.

# VITA

Edmund Yung Chen, the eldest son of Mr. and Mrs. Ching-Yu Chen, was born in Si-An, China on November 3, 1944. He received a Bachelor of Science degree in Mechanical Engineering from National Taiwan University in 1967.

He has been a graduate student in the School of Mechanical Engineering, Georgia Institute of Technology, since 1968. His thesis work was accomplished in the Metallurgy Division of the School of Chemical Engineering.

He married the former Rebecca Bei-Chia Yen in July, 1970, and has a son, Alexander I-Chung Chen, three years old.